

1 Responses of runoff to historical and future climate variability 2 over China

3 Chuanhao Wu¹, Bill X. Hu^{1,2*}, Guoru Huang^{3,4}, Peng Wang¹, and Kai Xu¹

4 ¹Institute of Groundwater and Earth Sciences, Jinan University, Guangzhou 510632, China.

5 ²Department of Earth, Ocean and Atmospheric Sciences, Florida State University, Tallahassee, FL, 32306, USA.

6 ³School of Civil Engineering and Transportation, South China University of Technology, Guangzhou 510640, China.

7 ⁴State Key Laboratory of Subtropical Building Science, South China University of Technology, Guangzhou 510640, China.

8 *Correspondence to:* Bill X. Hu (bill.x.hu@gmail.com)

9 **Abstract.** China has suffered some of the effects of global warming, and one of the potential implications of climate
10 warming is the alteration of the temporal-spatial patterns of water resources. Based on the long-term (1960–2008) water
11 budget data and climate projections from 28 Global Climate Models (GCMs) of the Coupled Model Intercomparison Project
12 Phase 5 (CMIP5), this study investigated the responses of runoff (R) to historical and future climate variability in China at
13 both grid and catchment scales using the Budyko-based elasticity method. Results show that there is a large spatial variation
14 in precipitation (P) elasticity (from 1.1 to 3.2) and potential evaporation (PET) elasticity (from -2.2 to -0.1) across China.
15 The P elasticity is larger in northeast and western China than in southern China, while the opposite occurs for PET elasticity.
16 The catchment properties elasticity of R appears to have a strong non-linear relationship with the mean annual aridity index
17 and tends to be more significant in more arid regions. For the period 1960–2008, the climate contribution to R ranges from
18 $-2.4\% \text{ yr}^{-1}$ to $3.6\% \text{ yr}^{-1}$ across China, with the negative contribution in northeast China and the positive contribution in
19 western China and some parts of the southwest. The results of climate projections indicate that although there is large
20 uncertainty involved in the 28 GCMs, most project a consistent change in P (or PET) in China at the annual scale. For the
21 period 2071–2100, the mean annual P is projected to increase in most parts of China, especially the western regions, while
22 the mean annual PET is projected to increase in all of China, particularly the southern regions. Furthermore, greater
23 increases are projected for higher emission scenarios. Overall, due to climate change, the arid regions and humid regions of
24 China are projected to become wetter and drier in the period 2071–2100, respectively (relative to the baseline 1971–2000).

25 **Key words:** Runoff; Budyko hypothesis; climate elasticity; climate variability; CMIP5 GCMs; China

26

27 1 Introduction

28 Climate change has become increasingly significant (IPCC, 2013), and numerous studies have reported that climate warming
29 is likely leading to the alteration of the hydrological cycle (Oki and Kanae, 2006; Jung et al., 2010). The dynamic properties
30 of the hydrological cycle are governed by the interactions and feedbacks between atmospheric and land surface hydrologic

31 processes on a catchment scale. The potential consequences of anthropogenic climate change on the hydrological cycle have
32 received significant attention over the last two decades (Wang et al., 2012; IPCC, 2013).

33

34 Runoff (R), as a commonly adopted indicator of the hydrologic cycle, is critical to human lives and economic activities
35 (Milly et al., 2005). There is a great deal of previous work exploring the impact of climate variations on R , with the
36 motivation stemming from the region's vast resources (Christensen et al., 2004; Guo et al., 2009; Piao et al., 2010; Chen et
37 al., 2012; Harding et al., 2012; Wang et al., 2012; Xu et al., 2013b), dangers of flooding (Kay et al., 2006, 2009, 2012; Raff
38 et al., 2009; Liu et al., 2013; Xiao et al., 2013; Wang et al., 2013; Smith et al., 2014; Wu et al., 2014, 2015), and agricultural
39 water uses (Vano et al., 2010). The most common practices in these previous studies are to use the hydrological models
40 driven by the output from Global Climate Models (GCMs) to simulate the hydrological process (e.g., R) under future climate
41 change scenarios. However, the key issue faced by such studies is the need to convert coarse resolution GCM outputs to local
42 catchment-scale climatic variables at a higher spatial resolution to serve as the input to a hydrological model (Vano et al.,
43 2015; Wu et al., 2015). The impact assessments are resource intensive and usually subject to uncertainties related to the
44 choice of hydrological model, GCMs, emissions scenarios, and downscaling techniques (Vano et al., 2014, 2015).

45

46 With the uncertainty in R due to climate change, simple tools able to provide robust estimates of this impact are essential to
47 support policy and planning decisions. Climate elasticity, as an important indicator, provides a measure of sensitivity of the
48 changes in R due to the changes in climate. Schaake (1990) made the first attempt to introduce the concept of elasticity and
49 related the climate elasticity of R to precipitation (P). Since then numerous climate elasticity methods have been developed
50 for evaluating the hydrologic response to climate change all over the world (Schaake, 1990; Dooge et al., 1999;
51 Sankarasubramanian et al., 2001; Milly and Dunne, 2002; Fu et al., 2007; Zheng et al., 2009; Ma et al., 2010; Yang and Yang,
52 2011; Yang et al., 2014; Vano et al., 2015). Sankarasubramanian et al. (2001) provided a detailed category of climate
53 elasticity methods for modelling climate change impacts. One of the most common methods is to analytically derive the
54 sensitivity of R based on the Budyko hypothesis, due to its clear theory and that it does not rely on a large amount of data
55 (Yang and Yang, 2011). More importantly, the Budyko-based elasticity method can derive the climate elasticity and can also
56 represent the impact of the catchment characteristics through the parameters of the Budyko model. Accordingly, it is widely
57 applied for the assessment of the hydrologic impacts of climate change (Dooge et al., 1999; Zheng et al., 2009; Yang and
58 Yang, 2011; Yang et al., 2014).

59

60 China is a vast land, spanning many degrees of latitude with complicated terrain, which results in a large regional variation
61 in climate elasticity. The investigation of the P elasticity of R has been reported in many regions of China, such as the Miyun

62 Reservoir basin (Ma et al., 2010), Luan River basin (Xu et al., 2013a), the headwater catchments of the Yellow River basin
63 (Zheng et al., 2009), Poyang Lake basin (Sun et al., 2013), and Hai River and Yellow River basins (Yang and Yang, 2011;
64 Liu and McVicar, 2012). Recently Yang et al. (2014) investigated the climate elasticity of R for the 210 catchments of China
65 based on the Budyko-based elasticity approach. The results indicated that the P elasticity exhibits a large regional variation,
66 with a small range in southern China, the Songhua River basin and the northwest and a large range in the Hai River basin,
67 the Yellow River basin, and the Liao River basin. Although the aforementioned studies have certainly made advances in
68 understanding the climate elasticity of R in China, our knowledge about the responses of R to climate change over various
69 temporal and spatial scales remains rather limited due to the large regional variation in climate types and catchment
70 characteristics. The question of how climate change will affect R over China in the future is also an important problem to be
71 addressed. Developing a more accurate and quantitative understanding of the changing water resources over various
72 temporal and spatial scales under a changing environment is therefore a high priority for China.

73

74 Based on the unique long-term (1960–2008) land surface dataset of China and the climate projections from 28 GCMs of the
75 Coupled Model Intercomparison Project Phase 5 (CMIP5), the objectives of this research are (1) to investigate the changes
76 of R and climate variables and their relationship at an interannual scale; (2) to estimate quantitatively the climate elasticity
77 and catchment properties elasticity of R across China at both grid and catchment scales; and (3) to predict climate change
78 and the changes in R due to future climate change for China from the CMIP5 projections at both grid and catchment scales.

79

80 **2 Data and methodology**

81 **2.1 Data sets**

82 Monthly data of potential evaporation (PET) covering the period 1960–2008 over China are provided by the
83 Hydroclimatology Group of Princeton University (Sheffield et al., 2006, 2012). The PET is estimated by the Penman
84 equation (Penman, 1948; Shuttleworth, 1993), using the updated meteorological dataset obtained from Sheffield et al. (2006,
85 2012). A long-term (1960–2008) daily land surface dataset over China, including P , surface runoff (RS), and baseflow (BS),
86 with a 0.25 degree spatial resolution were obtained from the Land Surface Processes and Global Change Research Group
87 (Zhang et al., 2014). In this dataset, P is driven by interpolating gauged daily precipitation from 756 meteorological stations
88 of the Chinese Meteorological Administration (CMA). RS and BS are derived from the Variable Infiltration Capacity (VIC)
89 model forced by the gridded daily climate forcings (i.e. P , maximum and minimum temperature, and wind speed). VIC
90 model parameters, including the infiltration shape parameter, the second and third soil layer depths, and the three parameters
91 in the base flow scheme, were estimated by using an optimization algorithm of the multi-objective complex evolution of the
92 University of Arizona (Zhang et al., 2014). The simulated monthly RS and BS match well with the observations at the large

93 river basins in China (Zhang et al., 2014). Compared with the global product of a similar nature, this dataset provides a more
 94 reliable estimate of land surface variables over China (Nijssen et al., 2001; Adam et al., 2006; Rodell et al., 2004; Sheffield et
 95 al., 2006; Sheffield and Wood, 2007; Pan et al., 2012). In this study, the data of P , RS , and BS are initially regridded onto 0.5°
 96 grids over China using the linear interpolation method. All the daily data (P , RS , and BS) and monthly data (PET) are then
 97 aggregated temporally for the annual scale over China. The R was calculated by the sum of RS and BS at each of the 0.5° grid
 98 points.

99
 100 Climate projections from 28 CMIP5 GCMs (as shown in Table 1) are provided by the Canadian Climate Data and Scenarios
 101 (CCDS, <http://www.cccsn.ec.gc.ca/index.php?page=gridded-data>). These data, including simulations of surface air
 102 temperature (T), P , sea ice thickness, sea ice concentration, snow depth, and near-surface wind speed, are statistically
 103 downscaled and regridded onto a common $1^\circ \times 1^\circ$ global grid by the CCDS. In this study, monthly P and monthly T over
 104 China, including one historical simulation for the period 1971–2000 and three emission scenarios (RCP2.6, RCP4.5, and
 105 RCP8.5) for the future period 2071–2100 from each of the 28 CMIP5 models and the multi-model ensemble of 28 CMIP5
 106 models, are used for the projections of climate change. The data are initially disaggregated to 0.5° grids over China then
 107 corrected by using a ‘delta change’ method (Wu et al., 2016), on the basis of the observed data of P and T as provided by the
 108 Climatic Research Unit (CRU) of the University of East Anglia (Harris et al., 2014).

109
 110 Figure 2 shows the comparison of observed mean annual T and P and the corresponding simulations from 28 CMIP5 models
 111 before and after bias correction for the 14 basins in China. The basin number is consistent with that given in Figure 1. As
 112 shown, the uncorrected model simulations tend to underestimate T and overestimate P for most of the basins, with more
 113 uncertainties for the simulation of P than for T . Compared to the uncorrected model results, the bias correction results
 114 represent large improvements and show a good agreement with the observed values for these basins. Therefore, the bias
 115 correction model simulations are acceptable for the investigation of climate change projections in this study.

116
 117 As the GCM data used only consist of P and T , the PET of GCM is estimated by the Thornthwaite method (Thornthwaite,
 118 1948) and then corrected by a multiplicative bias correction method as follows:

$$119 \quad PET_{cor,GCM,i} = PET_{Th,GCM,i} \times \frac{\overline{PET}_{Pen,obs,i}}{\overline{PET}_{Th,obs,i}} \quad (1)$$

120 where $PET_{cor,GCM,i}$ and $PET_{Th,GCM,i}$ are bias-corrected annual PET and the PET calculated from the Thornthwaite method,
 121 respectively, for the i th grid point of the GCMs. $\overline{PET}_{Pen,obs,i}$ and $\overline{PET}_{Th,obs,i}$ are the 49-year (1960–2008) averages of
 122 PET calculated from the Penman and Thornthwaite methods, respectively, for the i th grid point.

123

124 Based on the T data from the CRU, the Thornthwaite method is used to calculate PET to test the applicability of Equation (1).
 125 Figure 3 shows a comparison of annual PET calculated from the Penman method and that from the Thornthwaite method
 126 corrected by Equation (1) during the period 1960–2008. It is clear that the corrected PET agrees well with the PET from the
 127 Penman method, with the correlation coefficients of 0.94 and 0.958 at the catchment and grid scales, respectively. This
 128 suggests that Equation (1) can be acceptable for the bias correction of PET in the GCMs.

129

130 2.2 Sensitivity of runoff to climate and catchment properties

131 The Budyko framework has been widely used to study basin-scale water and energy balances. Two of the one-parameter
 132 formulations of the Budyko curve proposed by Choudhury (1999) (Equation (2), see also Yang et al., 2008) and Fu (1981)
 133 (Equation (3), see also Zhang et al., 2004) are expressed as:

$$134 \quad E = P \frac{PET}{(P^n + PET^n)^{1/n}}, \quad n \in (0, \infty) \quad (2)$$

$$135 \quad E = P + PET - (P^\omega + PET^\omega)^{1/\omega}, \quad \omega \in (1, \infty) \quad (3)$$

136 where n and ω are empirical parameters, representing the effects of other factors (e.g. land surface characteristics, the
 137 average slope, vegetation type or land use, and climate seasonality) on the water-energy balance (Yang et al., 2008, 2014;
 138 Roderick and Farquhar, 2011; Li et al., 2013a). Yang et al. (2008) calibrated the parameters n and ω using long-term water
 139 balance data from 108 catchments from the nonhumid regions of China and found that these two empirical parameters are
 140 linearly correlated.

141

142 Based on the Budyko hypothesis and assuming steady state conditions, Roderick et al. (2011) and Yang and Yang (2011)
 143 derived the elasticity method to estimate the contribution to R from the changes in climate (represented by P and PET) and
 144 catchment properties as follows:

$$145 \quad \frac{dR}{R} = \varepsilon_P \cdot \frac{dP}{P} + \varepsilon_{PET} \cdot \frac{dPET}{PET} + \varepsilon_n \cdot \frac{dn}{n} \quad (4)$$

146 where ε_P , ε_{PET} , and ε_n represent the elasticity coefficients of P , PET , and catchment properties respectively, and are
 147 expressed as:

$$148 \quad \varepsilon_P = \frac{P}{R} \left(1 - \frac{\partial E}{\partial P}\right) \quad (5a)$$

$$149 \quad \varepsilon_{PET} = -\frac{PET}{R} \frac{\partial E}{\partial PET} \quad (5b)$$

150

$$\varepsilon_n = -\frac{n}{R} \frac{\partial E}{\partial n} \quad (5c)$$

151

where $\frac{\partial E}{\partial P}$, $\frac{\partial E}{\partial PET}$, and $\frac{\partial E}{\partial n}$ denote the first order partial derivatives of the Budyko equation with respect to P , PET , and

152

the parameter n . In this study, both Equations (2) and (3) are used for the estimation of the elasticity of P , PET , and

153

catchment properties over China.

154

155

2.3 Trend estimate method

156

The Mann-Kendall (M-K) nonparametric test (Mann, 1945; Kendall, 1975) is an effective tool for detecting the statistical

157

significance of trends in the time series of meteorological and hydrological variables (Yang et al., 2014; Wu and Huang,

158

2015). In this study, the M-K method is used to detect the significance of monotonic trends in hydroclimatic time series. The

159

nonparametric trend slope estimator developed by Sen (1968) is used for the magnitude estimation of the trends in a

160

hydroclimatic time series.

161

162

3 Results

163

3.1 Interannual variability of climatic variables and runoff

164

The standard deviations for annual P , PET , and R are computed for each of the 0.5° grids in China, and the PET deviation

165

ratio (σ_{PET}/σ_P) and the R deviation ratio (σ_R/σ_P) are calculated. The spatial distributions of PET deviation ratio and R

166

deviation ratio across China are displayed in Figure 4(a) and (b). As shown, the PET deviation ratio is rather small in most

167

parts of China, especially the southern regions, while a larger value is observed mainly in the Xinjiang region, where there

168

are greater aridity indices. Generally, atmospheric water is enough to accommodate the limited PET in humid climates,

169

which would lead to a limited response of PET to P variability. Specifically, the interannual variability of PET is more

170

sensitive to that of P in arid climates (with water limits) than in humid climates (with energy limits). In contrast to the PET

171

deviation ratio, the R deviation ratio tends to increase from arid climates to humid climates. The reason for this is that, in arid

172

climates, the catchment water supply is very limited and gives priority to evaporation and soil storage capability, which leads

173

to little variation in R .

174

175

Figure 4(c) shows the relationship between the R deviation ratio and mean annual aridity index ($\bar{\phi}$) for all 0.5° grids in

176

China. As indicated, $\bar{\phi}$ is a major control for the R deviation ratio under not very dry conditions (e.g. $\bar{\phi} < 10$); that is, the R

177

deviation ratio decreases with increased $\bar{\phi}$. However, under very dry conditions (e.g. $\bar{\phi} > 10$) the R deviation ratio becomes

178 insensitive to $\bar{\phi}$, since in this case, other factors, such as soil storage capacity, can also have a large impact on the variation
179 of R .

180

181 3.2 Sensitivity of runoff to climate and catchment properties

182 3.2.1 Climate elasticity

183 The P elasticity and PET elasticity of R based on Equations (2) and (3) are estimated at each of the 0.5° grids in China. As
184 shown in Figure 5, the spatial patterns of P elasticity and PET elasticity from Equations (2) and (3) are almost the same in all
185 regions of China. There is a large spatial variation in P elasticity and PET elasticity, i.e. ranging from 1.1 to 3.2 and from
186 -2.2 to -0.1 across China, respectively. In particular, P elasticity is more significant in the northeast and western areas than in
187 southern China, which is in contrast to PET elasticity. Figure 6 shows the relationship between $\bar{\phi}$ and climate (P and PET)
188 elasticity. As shown, the P (PET) elasticity first increases (decreases) and then decreases (increases) with the increase of $\bar{\phi}$
189 under not very dry conditions (i.e. $\bar{\phi} < 10$). However, when $\bar{\phi}$ becomes large enough (e.g. $\bar{\phi} > 10$), both P and PET
190 elasticity becomes insensitive to $\bar{\phi}$.

191

192 The climate elasticity estimated for each of the 14 large basins is shown in Table 2. The values of P elasticity are in the range
193 of 1.39–2.28, with a larger (~smaller) elasticity in the Haihe River and Inner Mongolia River (Southwest Drainage). A
194 similar phenomenon is found for PET elasticity, which suggests that Haihe River (Southwest Drainage) is the most (least)
195 sensitive to PET among the 14 basins. Overall the values of P elasticity and PET elasticity derived by Equation (2) are very
196 close to those from Equation (3), but the difference between them tends to be larger for dry basins with increasing aridity
197 indices.

198

199 By using the estimates of climate elasticity derived by Equation (2), the change in R as a function of the percentage change
200 in P and PET is calculated for the 14 basins (Figure 7). The R is positively related to P and negatively related to PET , and the
201 magnitudes and patterns of the response of R to changes in P and PET vary in different scales. Generally, the R is more
202 sensitive to climate in the Haihe River and Inner Mongolia River, while relatively weak sensitivity is found in the Southwest
203 Drainage and Yangtze.

204

205 3.2.2 Catchment properties elasticity

206 The spatial distributions of catchment properties elasticity from Equations (2) and (3) are displayed in Figure 5(e) and (f). As
207 shown, the catchment properties elasticities for these two equations are rather similar across China, and the values of

208 Equation (3) are generally smaller than those from Equation (2). Regarding the spatial pattern, the catchment properties
209 elasticity is very weak (approximately equal to 0) in southern China and some regions of northeast China, but it tends to be
210 more significant in some water-limited regions of northwest China. Figure 6(c) shows the relationship between $\bar{\phi}$ and the
211 parameter elasticity for all 0.5° grids in China. It suggests that $\bar{\phi}$ is a major control for catchment properties elasticity
212 across China, i.e. the catchment properties elasticity would become stronger with increasing aridity indices. The catchment
213 properties elasticities estimated for the 14 large basins are shown in Table 2. The catchment properties elasticity shows a
214 large spatial variation, ranging from -2.78 to -0.24 for Equation (2) and from -4.3 to -0.33 for Equation (3). Overall, the
215 changes in R are more sensitive to catchment properties in arid basins with larger aridity indices, which is consistent with the
216 findings at the grid scale.

217

218 3.3 Climate change during 1960–2008

219 The annual trend magnitudes in P , R , PET , and aridity index during the period 1960–2008 are shown in Figure 8 (a), (b), (c),
220 and (d). As indicated, both P and R show an increasing trend mainly in the northwest and southeast regions and a decreasing
221 trend mainly in the central region and North China plain. A significant increasing in PET is detected mainly in northeast
222 China and eastern China, while the decreases mainly occur in most parts of western China. The aridity index tends to show
223 an increasing trend in most parts of China, indicating an increasing risk of meteorological drought in these regions during the
224 past several decades. In contrast, the decrease of aridity index is only found in some parts of western China.

225

226 3.4 Changes in runoff due to climate change during 1960–2008

227 Using the estimates of climate elasticity from Equation (2), the contributions of P , PET , and climate (i.e. $P \& PET$) to R in
228 China for the period 1960–2008 are calculated (as shown in Figure 8(e), (f), and (g)). A positive contribution (up to 3.7 %
229 yr⁻¹) from P to R is mainly recorded in western China, while a negative contribution is found mainly in northeast China and
230 North China plain. Negative and positive contributions of PET to R mainly occur in northeast China and western China,
231 respectively. The contributions of climate, i.e. the sum of the contributions from P and PET , ranges from -2.4 % yr⁻¹ to 3.6 %
232 yr⁻¹ across China. The spatial pattern of climate is rather similar to that of P , showing a negative contribution in northeast
233 China and a positive contribution in western China and some parts of the southeast. Particularly, the largest positive
234 contribution of climate occurs in the Tibetan plateau. The contributions of P , PET , and climate (i.e. $P \& PET$) to R in the 14
235 river basins for the period 1960–2008 are shown in Table 3. A positive contribution of P is detected in Southeast Drainage,
236 Southwest Drainage, Qiangtang, Qinghai, Xinjiang and Hexi, while an opposite contribution is found in other basins. In
237 contrast, a negative contribution of PET is found in most of the basins (except for Qiangtang and Hexi). In general, there is
238 an increased R in Southeast Drainage, Southwest Drainage, Qiangtang, Qinghai, Xinjiang and Hexi (from 0.06 to 1 % yr⁻¹)

239 and a decreased R in other basins (from -1.12 to -0.12 % yr⁻¹).

240

241 **3.5 Future climate change**

242 Figure 9 shows the uncertainty range of the relative change in mean annual P and PET in the basins for the period 2071–
243 2100 under the RCP2.6, RCP4.5, and RCP8.5 scenarios as predicted by 28 CMIP5 models (relative to the baseline 1971–
244 2000). As shown, there is a large difference between different GCMs and emission scenarios, which highlights the
245 uncertainty inherent in projections of climate change. However, overall P is projected to increase in most of the basins, and
246 greater increases are projected for higher emission scenarios. Meanwhile, greater increases tend to be projected for more arid
247 basins, suggesting a decreasing risk of meteorological drought in the future. The average changes (red dotted lines) of mean
248 annual P for the 14 basins range from 2.4 % to 11.0 % in RCP2.6, from 4.2 % to 16.0 % in RCP4.5, and from 3.1 % to 23.7 %
249 in RCP8.5. The largest increase in the RCP2.6 and RCP8.5 scenarios is found for the Qinghai River, while the largest
250 increase in the RCP4.5 scenario is projected for the Hexi River. For PET , there is an increase projected in all basins due to
251 climate warming, with the largest and smallest increases in the RCP8.5 and RCP2.6 scenarios, respectively. However, a large
252 uncertainty exists among the GCMs, which is similar to that for P . Furthermore, the uncertainty range tends to be larger with
253 higher emission scenarios. The average changes (red dotted lines) of PET for the basins range from 7.0 % to 12.0 % in
254 RCP2.6, from 13.5 % to 22.2 % in RCP4.5, and from 27.9 % to 49.8 % in RCP8.5. The largest and smallest average
255 increases are projected for the Pearl River and Qiangtang River, respectively.

256

257 Figure 10 displays the multi-model ensemble median relative change in mean annual P and PET in China for the period
258 2071–2100 (relative to the baseline 1971–2000). The projected changes in P (or PET) have a similar spatial pattern for the
259 three emission scenarios; that is, P is projected to show an increase in western China and the northeast, and PET is projected
260 to increase significantly in southern China and some parts of the Tibetan plateau, especially for the RCP8.5 scenario. In
261 addition, note that there are small changes in P and significant increases in PET projected for southern China. This would
262 result in an increasing risk of meteorological drought in the future.

263

264 **3.6 Future changes in runoff due to climate change**

265 Based on the estimates of elasticity from Equation (2), the percentage changes in the contributions of annual P and PET , as
266 well as climate, to R from the 28 GCMs for the period 2071–2100 are calculated for each of the 14 basins (relative to the
267 baseline 1971–2000). As shown in Figure 11, the changes in P contribution mainly follow the changes in P (Figure 9). A
268 positive contribution from P is projected for most of the basins, and larger contributions occur in more arid basins, as well as
269 in higher emission scenarios. Negative contributions of PET to R are projected for all basins due to the negative coefficients

270 of *PET* elasticity. Smaller contributions of *PET* are mainly found in the Southwest Drainage. In contrast, larger contributions
271 are projected mainly in the Huaihe River, Haihe River, and Inner Mongolia River, where the percentage decreases from the
272 28 models can be up to 25 %, 35 %, and 90 % in the RCP2.6, RCP4.5 and RCP8.5 scenarios, respectively.

273

274 Climate change is projected to reduce the *R* in some humid basins, such as the Southeast Drainage and Pearl River, where the
275 average changes in the three emission scenarios range from -22.83 % to -3.0 % and from -23.6 % to -3.5 %, respectively
276 (Figure 11 (g), (h) and (i)). For other basins, particularly for arid basins, the *R* is projected to increase due to climate change.
277 The largest average changes in *R* under the RCP2.6 and RCP4.5 scenarios are found in the Qinghai River (12.85 % and
278 16.18 %, respectively). For the RCP8.5 scenario, they are found in the Qiangtang River (18.59 %). Note that there is an
279 obvious decrease in *R* (-17.59 %) projected for the Huaihe River under RCP8.5 scenario, which is mainly caused by the
280 larger negative contribution of *PET*.

281

282 Figure 12 shows the spatial distributions of the relative changes in the contributions of annual *P* and *PET* as well as climate
283 to *R* in China for 2071–2100. This is based on the CMIP5 multi-model ensemble medians. Compared with the baseline
284 1971–2000, the increases in *R* due to the changes in *P* are projected in western China and some parts of northern China, and
285 this phenomenon is particularly significant in the RCP8.5 scenario (up to 60.3 %). In contrast, the changes in *PET* are
286 projected to reduce the *R* in all of China, with the larger decreases occurring mainly in the North China plain, northeast, and
287 some parts of western China. Overall, climate change is projected to cause an obvious increase (decrease) of *R* in western
288 China (southern China) under any emission scenario (Figure 12(g), (h) and (i)). This suggests that the arid regions (humid
289 regions) in China will become wetter (drier) in the future.

290

291 **4 Discussion**

292 **4.1 The estimation of elasticity**

293 The Budyko-based elasticity method is applied to quantify sensitivity of runoff to climate and catchment properties across
294 China. Two Budyko models proposed by Choudhury (1999) and Fu (1981) are used for the comparison of the estimation of
295 the climate elasticity of *R*. The results suggest that the climate elasticity is insensitive to the Budyko equations. The climate
296 elasticity of *R* has been estimated in many regions of China. For example, the values of *P* elasticity are estimated as 2.4 for
297 the Miyun Reservoir basin (Ma et al., 2010), 2.6 for the Luan River basin (Xu et al., 2013a), 2.1 for the headwater
298 catchments of the Yellow River basin (Zheng et al., 2009), 1.4–1.7 for the Poyang Lake basin (Sun et al., 2013), 1.7–3.1 for
299 the Hai River basin (Xu et al., 2014), 1.1–2.0 for southern China, the Songhua River basin, and the northwest, 2.1–4.8 for the
300 Hai River basin, the Yellow River basin, and the Liao River basin (Yang et al., 2014), and 1.6–3.8 for the 63 catchments of

301 China (Yang and Yang, 2011). In addition, the *PET* elasticity is estimated as -1.04 for the headwater catchments of the
302 Yellow River basin (Zheng et al., 2009) and from -1 to -0.2 for the Poyang Lake basin (Sun et al., 2013). Those results are
303 close to our results for *P* elasticity ranging from 1.1 to 3.2, and for *PET* elasticity ranging from -2.2 to -0.1 in China. It is
304 worth noting that the values of *P* elasticity tend to be larger in the northeast and some parts of western China that are located
305 in arid climates. This is in good agreement with the findings by Sankarasubramanian et al. (2001), which indicated that a
306 larger *P* elasticity occurs in more arid regions. However, some parts of Xinjiang, which is more arid than southern China,
307 have smaller *P* elasticity. Meanwhile, some parts of southern China, which is more humid than other regions in China, have
308 larger *P* elasticity (Figure 5). In addition, the Haihe River basin, located in less arid climates than that of the northwest,
309 shows the largest *P* elasticity in China (Table 2). A similar phenomenon is also introduced in Yang et al. (2014). One of the
310 major reasons for this difference may be attributed to the impacts of human activities that alter the patterns of *R* in these
311 regions. In addition, uncertainties in water budget data, such as the errors in the simulation of *R* and in the estimation of *PET*,
312 may also contribute to this difference.

313
314 The comparisons for the estimates of ε_n and ε_ω suggest that although the values of ε_n and ε_ω are mainly dependent on the
315 parameters of Budyko models, the spatial pattern of ε_n is consistent with that of ε_ω at the 0.5° grid points over China (Figure
316 5(e) and (f)). Yang et al. (2008) indicated that the parameters n and ω from Equations (2) and (3) are linearly correlated. We
317 also conducted a regression analysis of ε_n and ε_ω for all 0.5° grid points over China and found a strong linear correlation
318 between ε_n and ε_ω ($\varepsilon_\omega = 1.7061\varepsilon_n + 0.0986$, $r^2 = 0.96$). In addition, our results show that *R* is more sensitive to catchment
319 properties (ε_n and ε_ω) in the more arid regions (Figure 5(e) and (f)). The possible internal connection is that the arid regions
320 with less vegetation coverage and stronger evaporation do not effectively hold the rainfall water that will be evaporated,
321 leading to the smaller proportion of rainfall for *R*.

322 323 **4.2 Sensitivity analysis for *PET* calculation methods**

324 We compare four *PET* calculation methods, including the Penman method, the Thornthwaite method, the FAO-56 Penman–
325 Monteith method (Allen et al., 1998), and the Thornthwaite method corrected by Equation (1), to test the robustness of the
326 *PET* elasticity result subject to *PET* uncertainties. In terms of mean annual *PET* as shown in Figure 13 (a), the Thornthwaite
327 method gives relatively low *PET* among the four methods, especially in arid basins (e.g., Qiangtang, Qinghai, Xinjiang and
328 Hexi). This is in agreement with previous studies, which indicated that the Thornthwaite method tends to underestimate *PET*
329 in the arid areas (Hashemi and Habibian, 1979; Malek 1987; Garcia et al., 2004). In contrast, the mean annual *PET* by the
330 other three methods are quite consistent, especially for the Penman method and the Thornthwaite method corrected by
331 Equation (1). A similar result was also reported by Zeng and Cai (2016), which indicated that estimations of water balance at

332 both annual and month scales are generally robust under various *PET* calculation methods (not including the Thornthwaite
333 method). The *PET* elasticity calculations from the four different *PET* data for the 14 river basins are shown in Figure 13(b).
334 The Thornthwaite method yields stronger *PET* elasticity than other three methods in most of the basins mainly due to the
335 underestimation of *PET*. However, the other three methods give very similar results in all 14 basins. In summary, the
336 estimation of *PET* elasticity is robust to the *PET* calculations from the Penman method, the FAO-56 Penman–Monteith
337 method, and the Thornthwaite method corrected by Equation (1), but is not acceptable for the Thornthwaite method.

338

339 In general, the Thornthwaite method corrected by Equation (1) significantly improves the accuracy of *PET* (Figure 3 and
340 Figure 13(a)). However, it should be emphasized that the Thornthwaite method is an empirical equation that neglects the
341 effects of atmospheric conditions, such as wind speed, humidity and radiation (McVicar et al., 2012). In addition, the
342 Equation (1) used for the bias correction of *PET* belongs to a ‘delta method’ (Graham et al., 2007; Sperna Weiland et al.,
343 2010), which only considers the average change but ignores the differences in the standard deviation and the coefficient of
344 variation between the projection and baseline periods (Watanabe et al., 2012). Therefore, a more physically-based *PET*
345 calculation method (such as the Penman method) needs to be considered to fully understand the *PET* calculation
346 uncertainties in the projections of climate change.

347

348 **4.3 The projections of climate change and runoff**

349 The hydrological impacts of climate change have been investigated in many regions of China, such as the Hanjiang basin
350 (Chen et al., 2007; Guo et al., 2009), the catchment of the Loess Plateau (Wang et al., 2013), the Qingjiang River basin
351 (Chen et al., 2012), the Qiantang River basin (Xu et al., 2013b), the Songhuajiang River basin (Su et al., 2015), the
352 southeastern Tibetan Plateau (Li et al., 2013b), the Pearl River basin (Yan et al., 2015), the Xin River basin (Zhang et al.,
353 2016), the sub-catchments of the Yangtze and Yellow River basins (Xu et al., 2011), the Huang-Huai-Hai region (Lu et al.,
354 2012), and ten major river basins in China (Wang et al., 2012). There is a large uncertainty involved in these impact studies,
355 which results in a large difference in climate projections. For example, Wang et al. (2012) indicated that the prevailing
356 pattern of “north dry and south wet” in China will likely be exacerbated under future climate warming. However, the results
357 of most GCMs in this study suggest that the arid regions and humid regions of China are projected to become wetter and
358 drier in the future, respectively. The main difference between the two studies is the use of different climate models, emission
359 scenarios, and time periods. This also demonstrates that the results of climate projections should be taken with caution, since
360 the regional climate simulations (especially of precipitation) from the GCMs are still not robust at the present stage.

361

362 This study focuses on the hydrological change due to climate change (i.e., changes in *P* and *PET*), while the effects of the

363 variability of catchment properties (e.g., land cover change, groundwater and river water extraction, urbanization, irrigation,
364 etc.) on the hydrology are overlooked here. Most of the available GCMs lack of key regional feedback processes involving
365 land use, such as forest plantations, irrigation, and urbanization feedbacks that are critically important throughout China
366 (Piao et al., 2010). The projected changes in catchment properties therefore need to be involved in the GCMs to account for
367 their hydrological impacts. In addition, recent studies indicated that plant responses to increasing CO₂ tend to keep more
368 water on land, hence resulting in a greater increase in R (Milly and Dunne, 2016; Swann et al, 2016). That is to say, the
369 hydrological models (e.g., VIC model), without the schemes of the plant stomatal responses to CO₂, would lead to an
370 underestimation of R under high CO₂. Therefore, the implications of plants needing less water under high CO₂ should be
371 included in the assessment of hydrological impacts of climate change.

372

373 **4.4 Uncertainties**

374 Generally, a multitude of sources of uncertainty are involved in the impact assessment of climate change. In this study,
375 uncertainty mainly comes from the GCMs, emission scenarios, the elasticity method, and the estimation error of the water
376 budget data. To highlight the uncertainty from the GCMs, the 28 GCMs as produced by different research institutes around
377 the world, are used for the comparison of climate change projections. There exists a large difference in the projections of P
378 and PET among the 28 GCMs. Particularly, the uncertainty range of P tends to be larger for more arid regions, while the
379 uncertainty range of PET tends to be larger for more humid regions (Figure 9). This highlights the impact of potential
380 misleading conclusions if only one climate model were to be used for the impact assessments. The large uncertainty driven
381 by the GCMs in relation to the hydrological impacts of climate change has been reported in many previous studies (Kay et
382 al., 2009; Prudhomme and Davies, 2009; Chen et al., 2011; Teng et al., 2012; Liu et al., 2013; Wu et al., 2014, 2015). It is
383 worth noting that although the projected ranges of P and PET show large variability in various GCMs, most project a
384 consistent change (i.e. increase) in P and PET for the future period (Figure 9). In contrast, the uncertainty from the emission
385 scenarios is smaller than that from the GCMs, since the projected changes in P (or PET) show a similar pattern under all
386 emission scenarios (Figure 9). The main difference is that the projected changes tend to be more significant in higher
387 emission scenarios.

388

389 The elasticity equation (i.e. Equation (4)) used in this study is driven from the linear approximation of the Budyko equation
390 (Equations (2) and (3)) by neglecting the higher order. Such approximation would possibly lead to an uncertainty in the
391 estimation of climate elasticity. Yang et al. (2014) indicated that the error in estimation of elasticity tends to increase with
392 increasing changes in P and PET , as well as the increased parameter of the Budyko equation. Future research is needed to
393 quantify the effects of the errors on the estimation of elasticity under various climate conditions.

394

395 In addition to uncertainty in *PET* calculation (as discussed in section 4.2), there are also uncertainties associated with the
396 estimates of other water budget components, such as *R*. As shown in Figure 14, the sensitivity of climate (i.e., *P* and *PET*)
397 elasticity to *R* varies considerably between basins and tends to be larger in more humid basins. Moreover, *PET* elasticity is
398 more sensitive to changes in *R* compared with *P* elasticity for all 14 basins. As indicated by Zhang et al. (2014), although the
399 *R* is realistically estimated for most of the basins (especially for humid basins) in China with a small relative error, there is
400 still a large relative error for few arid basins in western China due to the lack of meteorological observations. Therefore, the
401 large errors in simulated *R* of the VIC model may result in large uncertainties in elasticity calculation, particularly in western
402 China. Also note that some other natural water sources, such as snow and glaciers, which may contribute to *R*, are
403 overlooked in this study. Lute and Abatzoglou (2014) highlighted the importance of extreme snowfall events in shaping the
404 interannual variability of the water balance. The melting of snow and glaciers is generally significant at a seasonal time scale
405 in some high altitude regions of China. Neglecting the effects of snow and glaciers would lead to a bias in the modelling of *R*
406 for these regions.

407

408 **5 Conclusion**

409 In this study, the Budyko-based elasticity method was used to investigate the responses of runoff to historical and future
410 climate variability over China at both grid and catchment scales. The climate and catchment properties elasticities of runoff
411 were estimated based on the long-term (1960–2008) land surface data from Zhang et al. (2014). Twenty-eight GCMs with
412 three emission scenarios from the CMIP5 were collected for the projections of climate change and its contribution to runoff
413 in China during the period 2071–2100. The uncertainties associated with the estimates of *PET*, *R*, climate elasticity, as well
414 as climate projections, are discussed in detail. The main findings are summarised as follows:

415

416 (1) The interannual variability of *PET* is more sensitive to that of *P* in more arid regions, while the opposite occurs in the
417 response of interannual variability of *R* to that of *P*. A large spatial variation exists in *P* elasticity (from 1.1 to 3.2) and *PET*
418 elasticity (from -2.2 to -0.1) across China. The *P* elasticity is larger in northeast and western China than in southern China,
419 which is opposite to that of *PET* elasticity. Among the 14 river basins, the Haihe River and Southwest Drainage have the
420 largest and smallest climate elasticities, respectively. The catchment properties elasticity of *R* is sensitive to mean annual
421 aridity indices and tends to be stronger in more arid regions with increasing aridity indices.

422

423 (2) For the period 1960–2008, the positive (negative) contributions from *P* to *R* are mainly found in western China (northeast
424 China and North China plain), and the positive (negative) contributions of *PET* mainly occur in western China (northeast

425 China). Overall, the climate contribution to R ranges from $-2.4 \% \text{ yr}^{-1}$ to $3.6 \% \text{ yr}^{-1}$ across China during the period 1960–
426 2008, with a negative contribution in northeast China and a positive contribution in western China and some parts of the
427 southwest. The largest positive and negative contributions of climate occur in the Qiangtang and Haihe River basins,
428 respectively.

429

430 (3) There is a large uncertainty in climate projections among the 28 GCMs. Moreover, the uncertainty range of the P (PET)
431 projection tends to be larger for more arid (humid) regions. However, most of the GCMs project a consistent change in
432 annual P or annual PET . For the period 2071–2100, the P is projected to increase in most parts of China, especially the
433 western regions, and the PET is projected to increase in all of China, particularly the southern regions. Furthermore, greater
434 increases are projected for higher emission scenarios. Due to future climate warming, the arid regions and humid regions of
435 China are projected to become wetter and drier in the period 2071–2100, respectively (relative to the baseline 1971–2000).

436

437 The results of this study (especially of the climate change projections) should be taken with caution, since uncertainties in
438 the results exist because of several issues, including the different simulations of GCMs, the estimation error of climate
439 elasticity, and the estimation error in the water budget components. A thorough investigation of the uncertainty involved in
440 the hydrologic effects of climate change in China should be considered in future research.

441

442 **Acknowledgements**

443 This research was supported by the Fundamental Research Funds for the Central Universities (Grant No. 21617301) and
444 partly supported by funding from the National Natural Science Foundation of China (Grant No. 41530316) and the National
445 Key Research and Development Program of China (Grant No. 2016YFC0402805).

446

447 **References**

448 Adam, J. C., Clark, E. A., Lettenmaier, D. P., and Wood, E. F.: Correction of global precipitation products for orographic
449 effects, *J. Climate.*, 19, 15–38, 2006.

450 Allen, R., Pereira, L., Raes, D., and Smith, M.: Crop evapotranspiration - Guidelines for computing crop water requirements,
451 FAO, Rome, 1998.

452 Chen, H., Guo, S. L., Xu, C. Y., and Singh, V. P.: Historical temporal trends of hydro-climatic variables and runoff response
453 to climate variability and their relevance in water resource management in the Hanjiang basin, *J. Hydrol.*, 344, 171–184,
454 doi:10.1016/j.jhydrol.2007.06.034, 2007.

455 Chen, H., Xiang, T. T., Zhou, X., and Xu, C. Y.: Impacts of climate change on the Qingjiang watershed's runoff change trend

456 in China, *Stochastic Environ. Res. Risk Assess.*, 26, 847–858, doi:10.1007/s00477-011-0524-2, 2012.

457 Chen, J., Brissette, F. P., Poulin, A., and Leconte, R.: Overall uncertainty study of the hydrological impacts of climate change
458 for a Canadian watershed, *Water Resour. Res.*, 47, W12509, doi:10.1029/2011WR010602, 2011.

459 Choudhury, B. J.: Evaluation of an empirical equation for annual evaporation using field observations and results from a
460 biophysical model, *J. Hydrol.*, 216 (1–2), 99–110, 1999.

461 Christensen, N. S., Wood, A. W., Voisin, N., Lettenmaier, D. P., and Palmer, R. N.: The effects of climate change on the
462 hydrology and water resources of the Colorado River basin, *Clim. Change*, 62(1-3), 337–363, 2004.

463 Dooge, J. C., Bruen, M., Parmentier, B.: A simple model for estimating the sensitivity of runoff to long-term changes in
464 precipitation without a change in vegetation, *Adv. Water Resour.*, 23 (2), 153–163, 1999.

465 Fu, B. P.: On the calculation of the evaporation from land surface, *Sci. Atmos.Sin.* 5 (1), 23–31, 1981. (in Chinese)

466 Fu, G., Charles, S. P., and Chiew, F. H.: A two-parameter climate elasticity of streamflow index to assess climate change
467 effects on annual streamflow, *Water Resour. Res.*, 43, W11419, doi:10.1029/2007WR005890, 2007.

468 Garcia, M., Raes, D., Allen, R., and Herbas, C.: Dynamics of reference evapotranspiration in the Bolivian highlands
469 (Altiplano), *Agricultural and forest meteorology*, 125(1), 67–82, 2004.

470 Graham, L. P., Andréasson, J., and Carlsson, B.: Assessing climate change impacts on hydrology from an ensemble of
471 regional climate models, model scales and linking methods—A case study on the Lule River basin, *Clim. Change*, 81(S1),
472 293–307, doi:10.1007/s10584-006-9215-2, 2007.

473 Guo S., Guo, J., Zhang, J., and Chen, H.: VIC distributed hydrological model to predict climate change impact in the
474 Hanjiang basin, *Sci. China Ser. E.*, 52, 3234–3239, 2009.

475 Harding, B. L., Wood, A. W., and Prairie, J. R.: The implications of climate change scenario selection for future streamflow
476 projection in the upper Colorado River basin, *Hydrol. Earth Syst. Sci.*, 16, 3989–4007, 2012.

477 Harris, I., Jones, P. D., Osborn, T. J., Lister, D. H.: Updated high-resolution grids of monthly climatic observations—the
478 CRU TS3.10 Dataset, *Int. J. Climatol.*, 34(3), 623–642, 2014.

479 Hashemi, F., Habibian, M. T.: Limitations of temperature-based methods in estimating crop evapotranspiration in arid-zone
480 agricultural projects. *Agric, Forest Meteorol.*, 20, 237–247, 1979.

481 IPCC: *Climate Change 2013: The Physical Science Basis. Contribution of Working Group I to the Fifth Assessment Report*
482 *of the Intergovernmental Panel on Climate Change*, edited by: Stocker, T. F., Qin, D., Plattner, G.-K., Tignor, M., Allen, S.
483 K., Boschung, J., Nauels, A., Xia, Y., Bex, V., and Midgley, P. M., Cambridge University Press, Cambridge, United
484 Kingdom and New York, NY, USA, 1535 pp, 2013.

485 Jung, M., and Coauthors: Recent decline in the global land evapotranspiration trend due to limited moisture supply, *Nature*,
486 467, 951–954, 2010.

487 Kay, A. L., Jones, R. G., and Reynard, N. S.: RCM rainfall for UK flood frequency estimation. II. Climate change results, *J.*
488 *Hydrol.*, 318, 163–172, doi:10.1016/j.jhydrol.2005.06.013, 2006.

489 Kay, A. L., Davies, H. N., Bell, V. A., and Jones, R. G.: Comparison of uncertainty sources for climate change impacts: flood
490 frequency in England, *Clim. Change*, 92, 41–63, 2009.

491 Kay, A. L. and Jones, D. A.: Transient changes in flood frequency and timing in Britain under potential projections of climate
492 change, *Int. J. Climatol.*, 32, 489–502, 2012.

493 Kendall, M. G.: *Rank Correlation Methods*, 4th edn. Charles Griffin: London, 1975.

494 Li, D., Pan, M., Cong, Z., Zhang, L., and Wood, E.: Vegetation control on water and energy balance within the Budyko
495 framework, *Water Resour. Res.*, 49, 969–976, doi :10.1002/wrcr.20107, 2013a.

496 Li, F., Zhang, Y., Xu, Z., Teng, J., Liu, C., Liu, W., and Mpelasoka, F.: The impact of climate change on runoff in the
497 southeastern Tibetan Plateau, *J. Hydrol.*, 505, 188–201, 2013b.

498 Liu, L. L., Fischer, T., Jiang, T., and Luo, Y.: Comparison of uncertainties in projected flood frequency of the Zhujiang River,
499 South China, *Quat. Int.*, 304, 51–61, 2013.

500 Liu, Q., and McVicar, T. R.: Assessing climate change induced modification of Penman potential evaporation and runoff
501 sensitivity in a large water-limited basin, *J. Hydrol.*, 464, 352–362, 2012.

502 Lu, G. H., Xiao, H., Wu, Z. Y., Zhang, S. L., and Li, Y.: Assessing the impacts of future climate change on hydrology in
503 Huang-Huai-Hai region in China using the PRECIS and VIC models. *J. Hydrol. Eng.*, 18(9), 1077–1087, 2012.

504 Lute, A. C., and Abatzoglou, J. T.: Role of extreme snowfall events in interannual variability of snowfall accumulation in the
505 western United States. *Water Resour. Res.* 50(4), 2874–2888, 2014.

506 Ma, H. A., Yang, D. W., Tan, S. K., Gao, B., Hu, Q. F.: Impact of climate variability and human activity on streamflow
507 decrease in the Miyun Reservoir catchment, *J. Hydrol.*, 389 (3–4), 317–324, 2010.

508 Malek, E.: Comparison of alternative methods for estimating ETP and evaluation of advection in the Bajah area, Iran. *Agric.*
509 *Forest Meteorol.*, 39, 185–192, 1987.

510 Mann, H. B.: Non-parametric tests against trend, *Econometrica* 13: 245–259, 1945.

511 McVicar, T.R., Roderick, M.L., Donohue, R.J., Li, L.T., Van Niel, T.G., Thomas, A., Grieser, J., Jhajharia, D., Himri, Y., and
512 Mahowald, N.M.: Global review and synthesis of trends in observed terrestrial near-surface wind speeds: implications for
513 evaporation, *J. Hydrol.* 416–417, 182–205, 2012.

514 Milly, P. C. D., and Dunne, K. A.: Macroscale water fluxes, 2. Water and energy supply control of their interannual
515 variability, *Water Resour. Res.*, 38(10), 1206, doi :10.1029/2001WR000760, 2002.

516 Milly, P. C., Dunne, K. A., and Vecchia, A. V.: Global pattern of trends in streamflow and water availability in a changing
517 climate, *Nature*, 438, 347–350, 2005.

518 Milly, P.C.D., and Dunne, K. A.: Potential Evapotranspiration and Continental Drying, *Nature Climate Change* 6:946–949,
519 2016.

520 Nijssen, B., Schnur, R., and Lettenmaier, D. P.: Global retrospective estimation of soil moisture using the Variable Infiltration
521 Capacity land surface model, 1980–93, *J. Climate.*, 14, 1790–1808, 2001.

522 Oki, T., and Kanae, S.: Global hydrological cycles and world water resources, *Science*, 313(5790), 1068–1072, 2006.

523 Pan, M., Sahoo, A. K., Troy, T. J., Vinukollu, R. K., Sheffield, J., and Wood, E. F.: Multisource estimation of long-term
524 terrestrial water budget for major global river basins, *J. Climate.*, 25, 3191–3206, 2012.

525 Penman, H. L.: Natural evaporation from open water, bare soil and grass. *Proc. Roy. Soc. Lond.* 193, 120–145, 1948.

526 Piao, S., and Coauthors: The impacts of climate change on water resources and agriculture in China, *Nature*, 467(7311), 43–
527 51, 2010.

528 Prudhomme, C. and Davies, H. N.: Assessing uncertainties in climate change impact analyses on river flow regimes in the
529 UK. Part 2: future climate, *Clim. Change*, 93, 197–222, 2009.

530 Raff, D. A., Pruitt, T., and Brekke, L. D.: A framework for assessing flood frequency based on climate projection information,
531 *Hydrol. Earth Syst. Sci.*, 13, 2119–2136, doi:10.5194/hess-13-2119-2009, 2009.

532 Rodell, M., and Coauthors: The Global Land Data Assimilation System, *Bull. Amer. Meteor. Soc.*, 85, 381–394, 2004.

533 Roderick, M. L., and Farquhar, G. D.: A simple framework for relating variations in runoff to variations in climatic
534 conditions and catchment properties, *Water Resour. Res.*, 47, W00G07, doi:10.1029/2010WR009826, 2011.

535 Roderick, M. L., Sun, F., Lim, W. H., and Farquhar, G. D.: A general framework for understanding the response of the water
536 cycle to global warming over land and ocean, *Hydrol. Earth Syst. Sci.*, 18, 1575–1589, 2014.

537 Sankarasubramanian, A., Vogel, R. M., and Limbrunner, J. F.: Climate elasticity of streamflow in the United States, *Water*
538 *Resour. Res.*, 37(6), 1771–1781, 2001.

539 Schaake, J. C.: From climate to flow. In: Waggoner (Ed.), *Climate Change and U.S. Water Resources*, John Wiley, New York,
540 pp. 177–206, 1990.

541 Sen P. K.: Estimates of the regression coefficient based on Kendall’s tau. *J. Am. Stat. Assoc.*, 63, 1379–1389, 1968.

542 Sheffield, J., Goteti, G., and Wood, E. F.: Development of a 50-year high-resolution global dataset of meteorological forcings
543 for land surface modeling, *J. Climate.*, 19, 3088–3110, 2006.

544 Sheffield, J., and Wood, E. F.: Characteristics of global and regional drought, 1950–2000: Analysis of soil moisture data
545 from off-line simulation of the terrestrial hydrologic cycle, *J. Geophys. Res.*, 112, D17115, doi: 10.1029/2006JD008288,
546 2007.

547 Sheffield, J., Wood, E.F., Roderick, M.L.: Little change in global drought over the past 60 years. *Nature*, 491, 435–438.
548 doi:10.1038/nature11575, 2012.

549 Shuttleworth, W.J.: Evaporation. In: Maidment, D.R. (Ed.), *Handbook of Hydrology*. McGraw-Hill, Sydney, 1993.

550 Smith, A., Bates, P., Freer, J., and Wetterhall, F.: Investigating the application of climate models in flood projection across the
551 UK, *Hydrol. Process.*, 28, 2810–2823, doi:10.1002/hyp.9815, 2014.

552 Sperna Weiland, F. C., van Beek, L. P. H., Kwadijk, J. C. J., and Bierkens, M. F. P.: The ability of a GCM-forced
553 hydrological model to reproduce global discharge variability, *Hydrol. Earth Syst. Sci.*, 14(8), 1595–1621, 2010.

554 Su, B., Zeng, X., Zhai, J., Wang, Y., and Li, X.: Projected precipitation and streamflow under sres and rcp emission scenarios
555 in the songhuajiang river basin, China, *Quatern. Int.*, 380, 95–105, 2015.

556 Sun, S.L., Chen, H.S., Ju, W.M., Song, J., Zhang, H., Sun, J., Fang, Y.J.: Effects of climate change on annual streamflow
557 using climate elasticity in Poyang Lake Basin, China, *Theor. Appl. Climatol.* 112 (1–2), 169–183, 2013.

558 Swann, A. L., Hoffman, F. M., Koven, C. D., and Randerson, J. T.: Plant responses to increasing CO₂ reduce estimates of
559 climate impacts on drought severity, *Proceedings of the National Academy of Sciences*, 113(36), 10019–10024, 2016.

560 Teng, J., Vaze, J., Chiew, F. H. S., Wang, B., and Perraud, J.: Estimating the Relative Uncertainties Sourced from GCMs and
561 Hydrological Models in Modeling Climate Change Impact on Runoff, *J. Hydrometeor.*, 13, 122–139, 2012.

562 Thornthwaite, C. W.: An approach toward a rational classification of climate, *Geographical Review*, 38, 55–94, 1948.

563 Vano, J. A., Scott, M., Voisin, N., Stockle, C. O., Hamlet, A. F., Mickelson, K. E. B., Elsner, M. M., and Lettenmaier, D. P.:
564 Climate change impacts on water management and irrigated agriculture in the Yakima River basin, Washington, USA, *Clim.*
565 *Change*, 102(1–2), 287–317, doi:10.1007/s10584-010-9856-z, 2010.

566 Vano, J. A., et al.: Understanding uncertainties in future Colorado River streamflow, *Bull. Am. Meteorol. Soc.*, 95, 59–78,
567 2014.

568 Vano, J. A., Nijssen, B., and Lettenmaier, D. P.: Seasonal hydrologic responses to climate change in the Pacific Northwest,
569 *Water Resour. Res.*, 51(4), 1959–1976, 2015.

570 Wang, D., and Alimohammadi, N.: Responses of annual runoff, evaporation, and storage change to climate variability at the
571 watershed scale, *Water Resour. Res.*, 48, W05546, doi:10.1029/2011WR011444, 2012.

572 Wang, G. Q., Zhang, J. Y., Jin, J. L., Pagano, T. C., Calow, R., Bao, Z. X., Liu, C. S., Liu, Y. L., and Yan, X. L.: Assessing
573 water resources in China using PRECIS projections and a VIC model, *Hydrol. Earth Syst. Sci.*, 16(1), 231–240, 2012.

574 Wang, G. Q., Zhang, J. Y., Xuan, Y. Q., Liu, J. F., Jin, J. L., Bao, Z. X., He, R. M., Liu, C. S., Liu, Y. L., and Yan, X. L.:
575 Simulating the impact of climate change on runoff in a typical river catchment of the Loess Plateau, China, *J. Hydrometeor.*,
576 14(5), 1553–1561, 2013.

577 Watanabe, S., Kanae, S., Seto, S., Yeh, P. J. F., Hirabayashi, Y., and Oki, T.: Intercomparison of bias-correction methods for
578 monthly temperature and precipitation simulated by multiple climate models, *J. Geophys. Res.*, 117(D23), 2012.

579 Wu, C. H., Huang, G. R., Yu, H. J., Chen, Z. J., and Ma, J. G.: Impact of climate change on reservoir flood control in the

580 upstream area of the Beijiang River Basin, South China, *J. Hydrometeor.*, 15, 2203–2218, doi:10.1175/JHM-D-13-0181.1,
581 2014.

582 Wu, C. H., Huang, G. R., and Yu, H. J.: Prediction of extreme floods based on CMIP5 climate models: a case study in the
583 Beijiang River basin, South China, *Hydrol. Earth Syst. Sci.*, 19(3), 1385–1399, 2015.

584 Wu, C. H., and Huang, G. R.: Changes in heavy precipitation and floods in the upstream of the Beijiang River basin, South
585 China, *Int. J. Climatol.*, 35(10), 2978–2992, 2015.

586 Wu, C. H., Xian, Z. Y., and Huang, G. R.: Meteorological drought in the Beijiang River basin, South China: current
587 observations and future projections, *Stoch. Environ. Res. Risk Assess.*, 30: 1821–1834, doi:10.1007/s00477-015-1157-7,
588 2016.

589 Xiao, H., Lu, G. H., Wu, Z. Y., and Liu Z. Y.: Flood response to climate change in the Pearl River basin for the next three
590 decades, *J. Hydraul. Eng.*, 12, 1409–1419, 2013. (in Chinese)

591 Xu, H., Taylor, R. G., and Xu, Y.: Quantifying uncertainty in the impacts of climate change on river discharge in
592 sub-catchments of the Yangtze and Yellow River Basins, China, *Hydrol. Earth Syst. Sci.*, 15, 333–344, 2011.

593 Xu, X.Y., Yang, H.B., Yang, D.W., Ma, H.: Assessing the impacts of climate variability and human activities on annual
594 runoff in the Luan River basin, China, *Hydrol. Res.*, 44 (5), 940–952, 2013a.

595 Xu, Y. P., Zhang, X., Ran, Q., and Tian, Y.: Impact of climate change on hydrology of upper reaches of Qiantang River Basin,
596 East China, *J. Hydrol.*, 483, 51–60, 2013b.

597 Xu, X. Y., Yang, D. W., Yang, H. B., Lei, H. M.: Attribution analysis based on the Budyko Hypothesis for detecting the
598 dominant cause of runoff decline in Haihe basin, *J. Hydrol.*, 510, 530–540, 2014.

599 Yan, D., Werners, S. E., Ludwig, F., and Huang, H. Q.: Hydrological response to climate change: The Pearl River, China
600 under different RCP scenarios, *Journal of Hydrology: Regional Studies*, 4, 228–245, 2015.

601 Yang, H., Yang, D., Lei, Z., and Sun, F.: New analytical derivation of the mean annual water-energy balance equation, *Water*
602 *Resour. Res.*, 44, W03410, doi:10.1029/2007WR006135, 2008.

603 Yang, H., and Yang, D.: Derivation of climate elasticity of runoff to assess the effects of climate change on annual runoff,
604 *Water Resour. Res.*, 47, W07526, doi:10.1029/2010WR009287, 2011.

605 Yang, H., Qi, J., Xu, X., Yang, D., and Lv, H.: The regional variation in climate elasticity and climate contribution to runoff
606 across China, *J. Hydrol.*, 517, 607–616, 2014.

607 Zhang, L., Hickel, K., Dawes, W. R., Chiew, F. H. S., Western, A. W., and Briggs, P. R.: A rational function approach for
608 estimating mean annual evapotranspiration, *Water Resour. Res.*, 40, W02502, doi:10.1029/2003WR002710, 2004.

609 Zhang, X., Tang, Q., Pan, M., Tang, Y.: A Long-Term Land Surface Hydrologic Fluxes and States Dataset for China, *J.*
610 *Hydrometeor.*, 15, 2067–2084, doi: 10.1175/JHM-D-13-0170.1, 2014.

611 Zhang, Y., You, Q., Chen, C., and Ge, J.: Impacts of climate change on streamflows under RCP scenarios: A case study in
612 Xin River Basin, China, *Atmospheric Research*, 178, 521–534, 2016.

613 Zheng, H., Zhang, L., Zhu, R., Liu, C., Sato, Y., and Fukushima, Y.: Responses of streamflow to climate and land surface
614 change in the headwaters of the Yellow River Basin, *Water Resour. Res.*, 45, W00A19, doi:10.1029/2007WR006665, 2009.

615 Zeng, R., Cai, X.: Climatic and terrestrial storage control on evaporation temporal variability: Analysis of river basins around
616 the world, *Geophys. Res. Lett.*, 43, doi:10.1002/2015GL066470, 2016.

617

618

619

620

621

622

623

624

625

626

627

628

629

630

631

632

633

634

635

636

637

638

639

640 **Table 1.** CMIP5 GCMs used in this study. The GCM data were statistically downscaled and regridded
 641 onto a common $1^{\circ}\times 1^{\circ}$ global grid by the Canadian Climate Data and Scenarios (CCDS).

No.	Model	Institution (Country)	Resolution
1	BCC-CSM1-1	Beijing Climate Center, China Meteorological Administration,	$1^{\circ}\times 1^{\circ}$
2	BCC-CSM1-1-m	China	
3	BNU-ESM	College of Global Change and Earth System Science, Beijing Normal University, China	$1^{\circ}\times 1^{\circ}$
4	CCSM4	National Center for Atmospheric Research, USA	$1^{\circ}\times 1^{\circ}$
5	CESM1-CAM5	Community Earth System Model Contributors, USA	$1^{\circ}\times 1^{\circ}$
6	CNRM-CM5	Centre National de Recherches Météorologiques / Centre Européen de Recherche et Formation Avancée en Calcul Scientifique, France	$1^{\circ}\times 1^{\circ}$
7	CSIRO-Mk3-6-0	Commonwealth Scientific and Industrial Research Organization in collaboration with Queensland Climate Change Centre of Excellence, Australia	$1^{\circ}\times 1^{\circ}$
8	CanESM2	Canadian Centre for Climate Modelling and Analysis, Canada	$1^{\circ}\times 1^{\circ}$
9	EC-EARTH	EC-EARTH consortium	$1^{\circ}\times 1^{\circ}$
10	FGOALS-g2	LASG, Institute of Atmospheric Physics, Chinese Academy of Sciences and CESS, Tsinghua University, China	$1^{\circ}\times 1^{\circ}$
11	FIO-ESM	The First Institute of Oceanography, SOA, China	$1^{\circ}\times 1^{\circ}$
12	GFDL-CM3		
13	GFDL-ESM2G	NOAA Geophysical Fluid Dynamics Laboratory, USA	$1^{\circ}\times 1^{\circ}$
14	GFDL-ESM2M		
15	GISS-E2-H		
16	GISS-E2-R	NASA Goddard Institute for Space Studies, USA	$1^{\circ}\times 1^{\circ}$
17	HadGEM2-AO	National Institute of Meteorological Research/Korea Meteorological Administration, South Korea	$1^{\circ}\times 1^{\circ}$
18	HadGEM2-ES	Met Office Hadley Centre (additional HadGEM2-ES realizations contributed by Instituto Nacional de Pesquisas Espaciais), UK	$1^{\circ}\times 1^{\circ}$
19	IPSL-CM5A-LR		
20	IPSL-CM5A-MR	Institut Pierre-Simon Laplace, France	$1^{\circ}\times 1^{\circ}$
21	MIROC-ESM	Japan Agency for Marine-Earth Science and Technology, Atmosphere and Ocean	$1^{\circ}\times 1^{\circ}$
22	MIROC-ESM-CHEM	Research Institute (The University of Tokyo), and National Institute for Environmental Studies, Japan	
23	MIROC5	Atmosphere and Ocean Research Institute (The University of Tokyo), National Institute for Environmental Studies, and Japan Agency for Marine-Earth Science and Technology, Japan	$1^{\circ}\times 1^{\circ}$
24	MPI-ESM-LR	Max-Planck-Institut für Meteorologie (Max Planck Institute for Meteorology), Germany	$1^{\circ}\times 1^{\circ}$
25	MPI-ESM-MR		
26	MRI-CGCM3	Meteorological Research Institute, Japan	$1^{\circ}\times 1^{\circ}$
27	NorESM1-M		
28	NorESM1-ME	Norwegian Climate Centre, Norway	$1^{\circ}\times 1^{\circ}$

643 **Table 2.** The estimations of P elasticity, PET elasticity, and catchment properties elasticity of R in the
644 14 river basins of China based on Equations (2) and (3). The basin number is consistent with that given
645 in Figure 1. The numbers in the parentheses indicate the 1960–2008 mean aridity index.

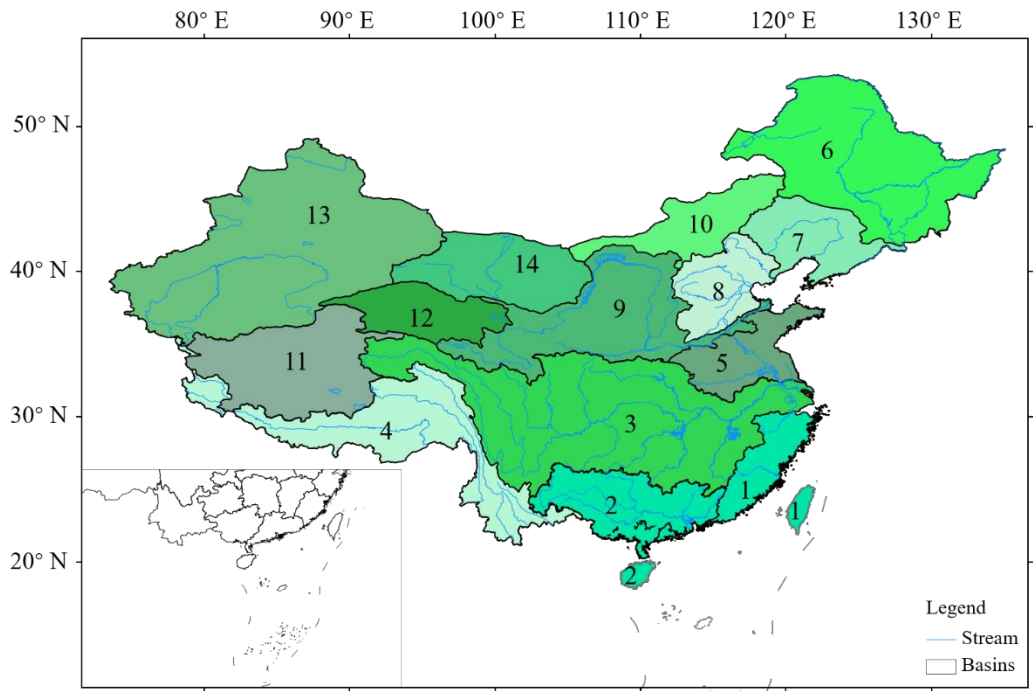
Basin No.	ε_P		ε_{PET}		ε_n OR ε_ω	
	Eq.(2)	Eq.(3)	Eq.(2)	Eq.(3)	Eq.(2)	Eq.(3)
1 (0.52)	1.64	1.65	-0.64	-0.65	-0.24	-0.33
2 (0.64)	1.63	1.64	-0.62	-0.63	-0.41	-0.61
3 (0.81)	1.55	1.56	-0.55	-0.55	-0.57	-0.93
4 (1.19)	1.40	1.39	-0.40	-0.39	-0.73	-1.44
5 (1.19)	2.09	2.08	-1.08	-1.07	-1.03	-1.47
6 (1.43)	2.06	2.04	-1.05	-1.02	-1.25	-1.83
7 (1.71)	1.92	1.88	-0.91	-0.87	-1.35	-2.10
8 (2.14)	2.28	2.21	-1.29	-1.22	-1.89	-2.70
9 (2.38)	1.78	1.72	-0.79	-0.73	-1.53	-2.54
10 (4.41)	2.23	2.11	-1.22	-1.10	-2.78	-4.16
11 (4.70)	1.81	1.72	-0.82	-0.72	-2.17	-3.67
12 (6.68)	1.72	1.62	-0.73	-0.63	-2.28	-4.08
13 (8.09)	1.66	1.56	-0.65	-0.55	-2.26	-4.27
14 (8.63)	1.63	1.53	-0.64	-0.54	-2.26	-4.30

646
647
648

649 **Table 3.** The contributions of P , PET , and climate (i.e. $P&PET$) to R in the 14 basins of China for the
650 period 1960–2008. The basin number is consistent with that given in Figure 1. The numbers in the
651 parentheses indicate the 1960–2008 mean aridity index.

Basin No.	P (%/a)	PET (%/a)	$P&PET$ (%/a)
1 (0.52)	0.19	-0.13	0.06
2 (0.64)	-0.03	-0.09	-0.12
3 (0.81)	-0.07	-0.07	-0.14
4 (1.19)	0.14	-0.01	0.13
5 (1.19)	-0.18	-0.27	-0.45
6 (1.43)	-0.35	-0.31	-0.66
7 (1.71)	-0.57	-0.34	-0.91
8 (2.14)	-0.74	-0.38	-1.12
9 (2.38)	-0.38	-0.04	-0.42
10 (4.41)	-0.40	-0.26	-0.66
11 (4.70)	0.99	0.01	1.00
12 (6.68)	0.43	-0.01	0.42
13 (8.09)	0.84	-0.02	0.82
14 (8.63)	0.11	0.08	0.19

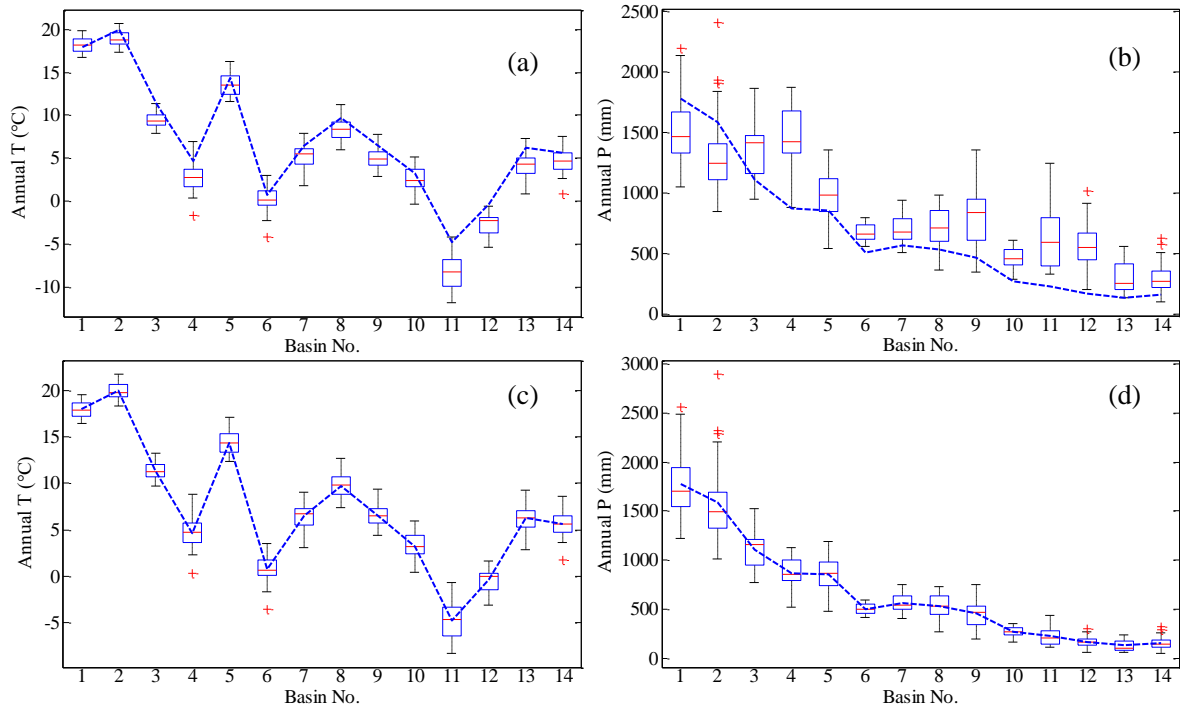
652
653
654



655

656 **Figure 1.** Location of the main river basins in China. The numbers denote the river basins with
 657 increasing aridity index: 1, Southeast Drainage (0.52); 2, Pearl River (0.64); 3, Yangtze River (0.81); 4,
 658 Southwest Drainage (1.19); 5, Huaihe River (1.19); 6, Heilongjiang River (1.43); 7, Liaohe River (1.71);
 659 8, Haihe River (2.14); 9, Yellow River (2.38); 10, Inner Mongolia River (4.41); 11, Qiangtang River
 660 (4.70); 12, Qinghai River (6.68); 13, Xinjiang River (8.09), 14, Hexi River (8.63). The numbers in the
 661 parentheses indicate the 1960–2008 mean aridity index.

662
 663
 664
 665
 666
 667
 668



669

670 **Figure 2.** Box plots of the simulation results of (a) mean annual T and (b) mean annual P and the bias
 671 correction results of (c) mean annual T and (d) mean annual P from 28 GCMs for the period 1971–2000
 672 in the 14 river basins. The boxes denote the interquartile model spread (range between the 25th and 75th
 673 quantiles), with the horizontal line indicating the ensemble median and the whiskers showing the
 674 extreme range of the 28 CMIP5 model simulations. The blue dotted lines denote the observed results of
 675 mean annual T and mean annual P for the period 1971–2000. The basin number is consistent with that
 676 given in Figure 1.

677

678

679

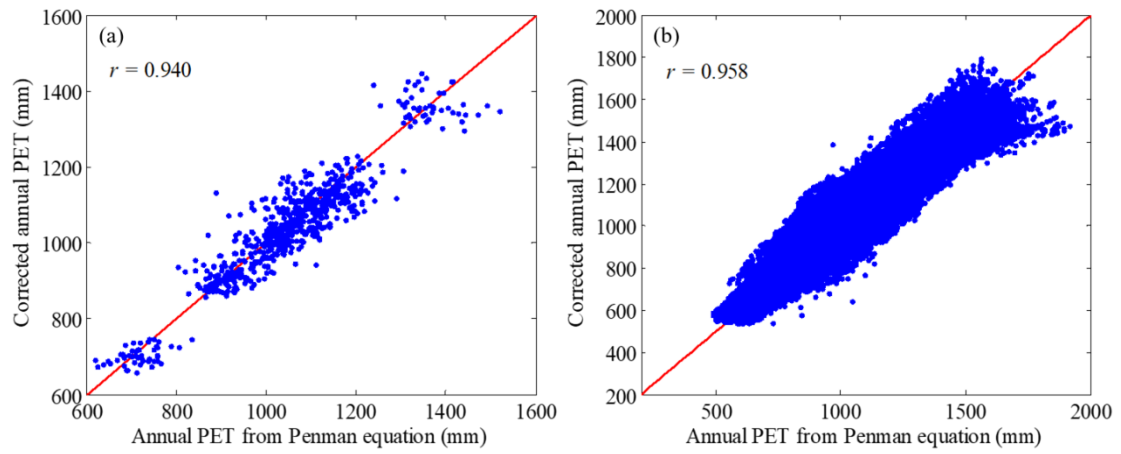
680

681

682

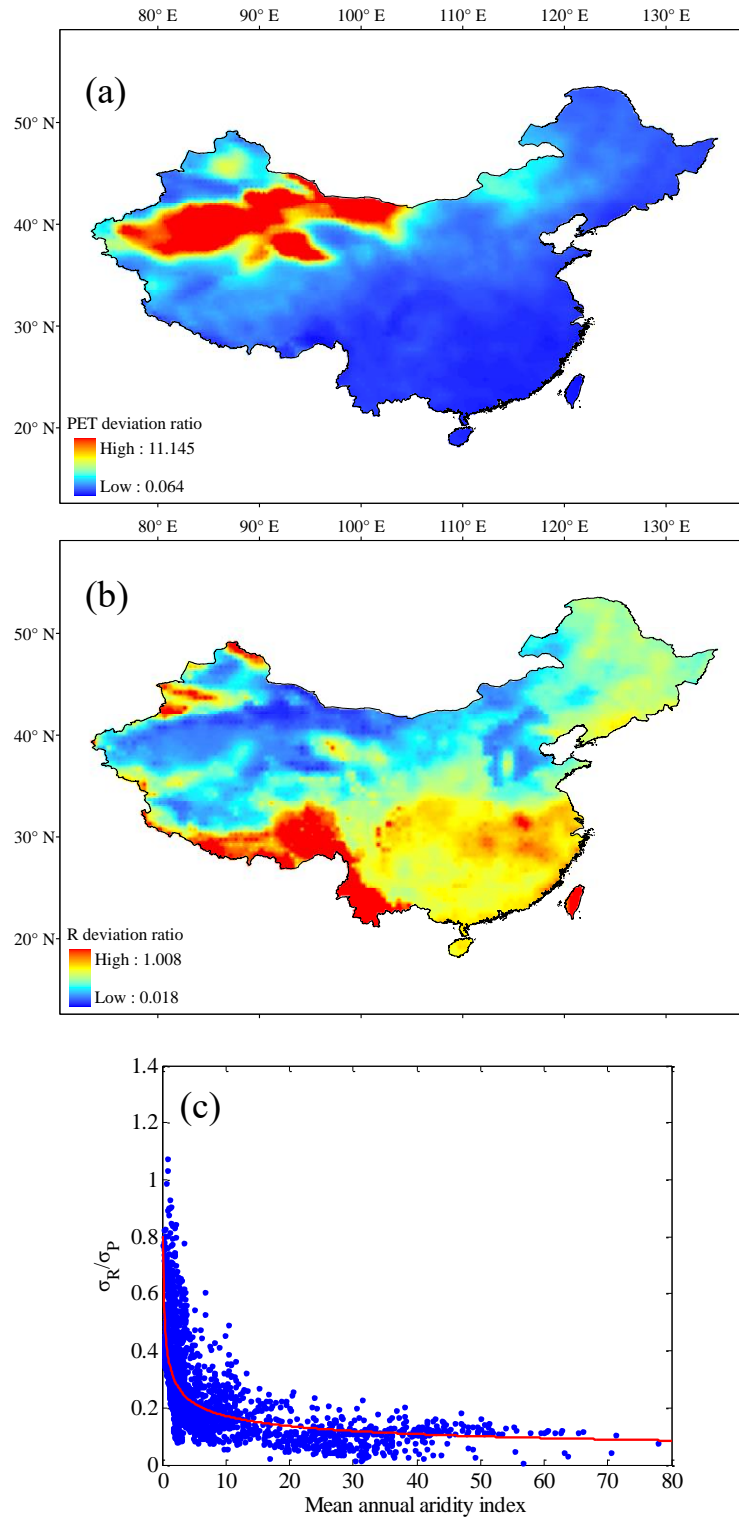
683

684



685

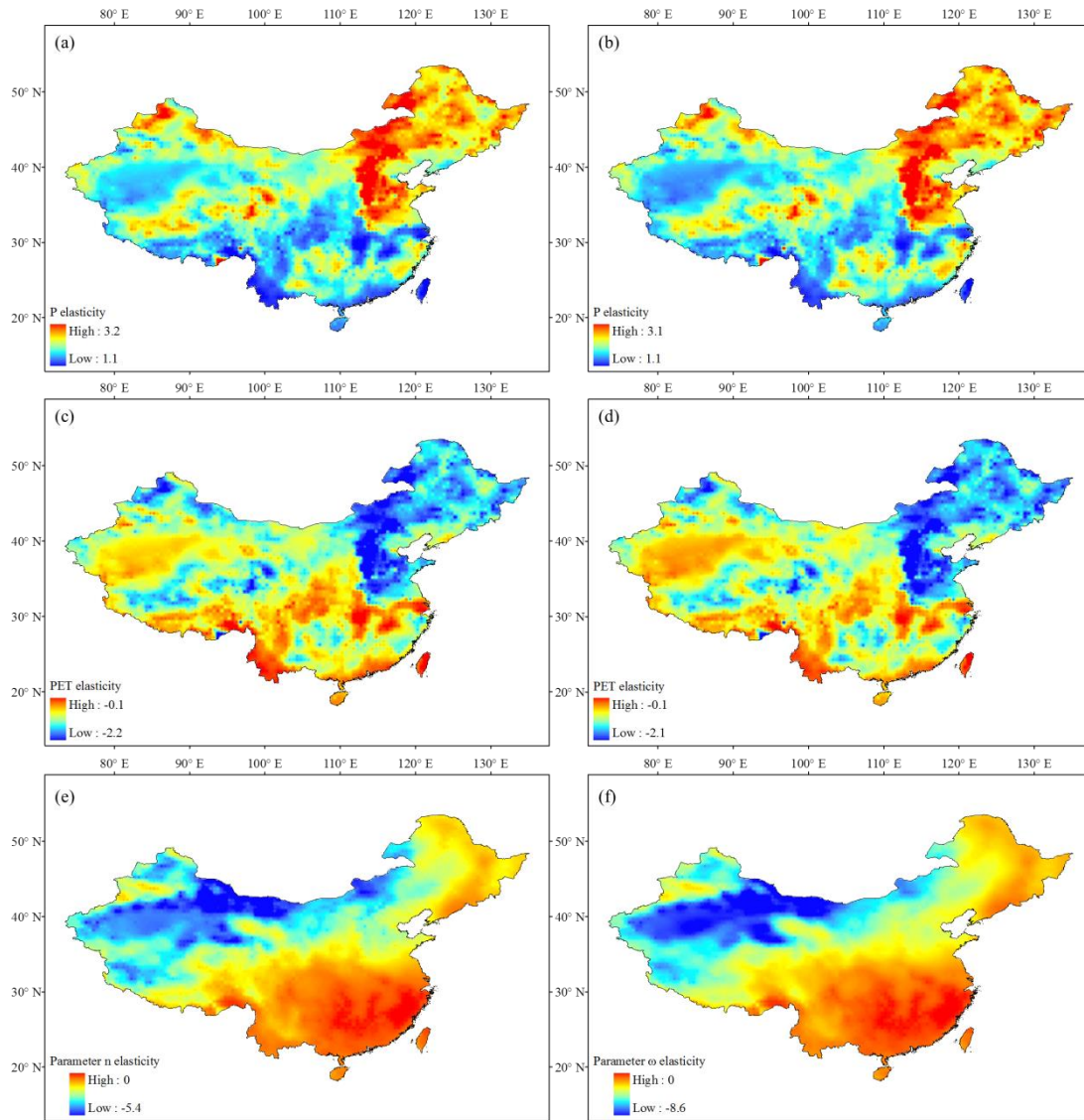
686 **Figure 3.** Comparison of annual *PET* calculated from the Penman method and the Thornthwaite method
 687 corrected by Equation (1) during the period 1960–2008 for (a) the 14 river basins and (b) all 0.5° grid
 688 points over China.



689

690 **Figure 4.** Spatial distributions of (a) *PET* deviation ratio and (b) *R* deviation ratio and (c) the
 691 relationship between *R* deviation ratio and mean annual aridity index ($\bar{\phi}$) for all 0.5° grid points in
 692 China.

693



694

695 **Figure 5.** Spatial distributions of the P elasticity of R across China from (a) Equation (2) and (b)
 696 Equation (3). Spatial distributions of the PET elasticity of R across China from (c) Equation (2) and (d)
 697 Equation (3). Spatial distributions of the parameter elasticity of R across China from (e) Equation (2)
 698 and (f) Equation (3).

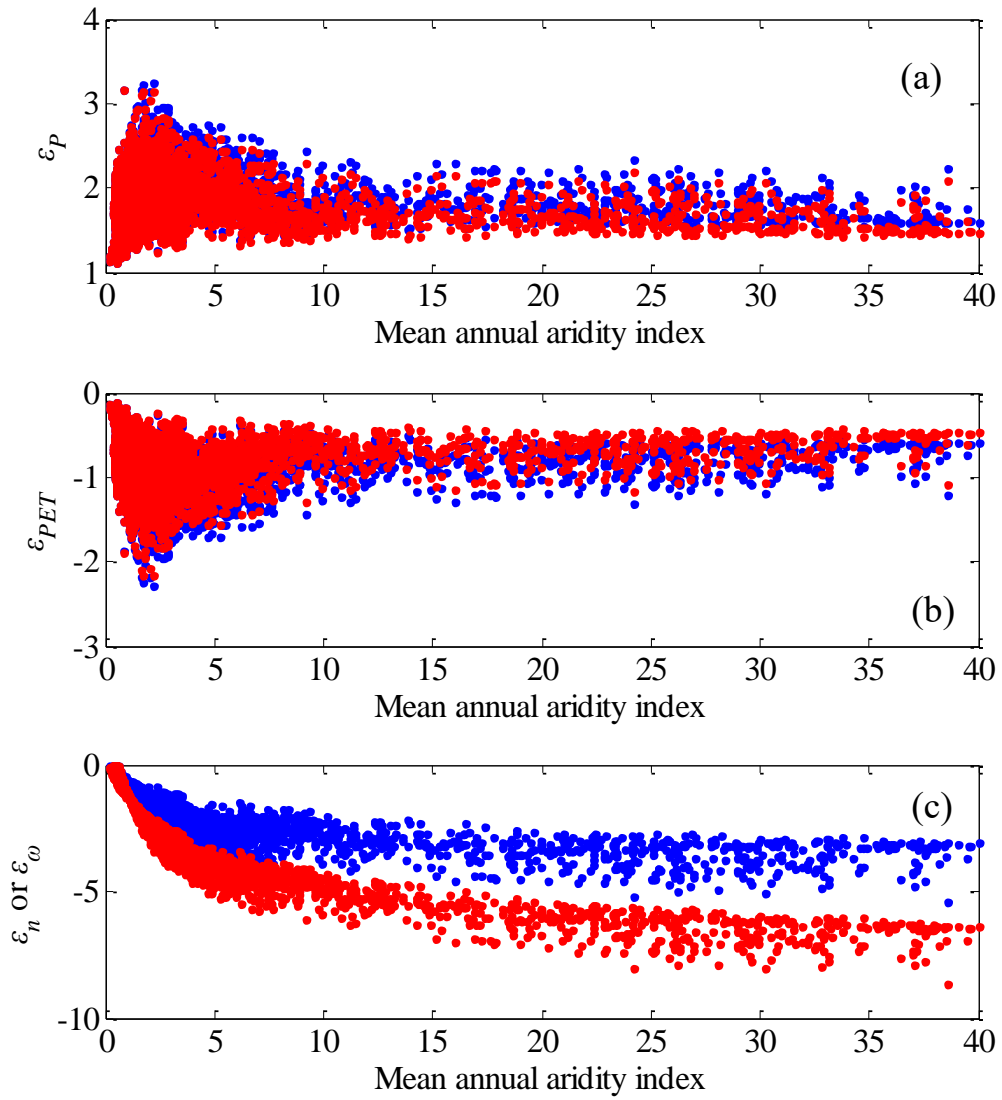
699

700

701

702

703



704

705 **Figure 6.** The relationship between mean annual aridity index and (a) P elasticity, (b) PET elasticity,
 706 and (c) parameter elasticity. The blue points represent the case of Equation (2), and the red points

707 represent the case of Equation (3).

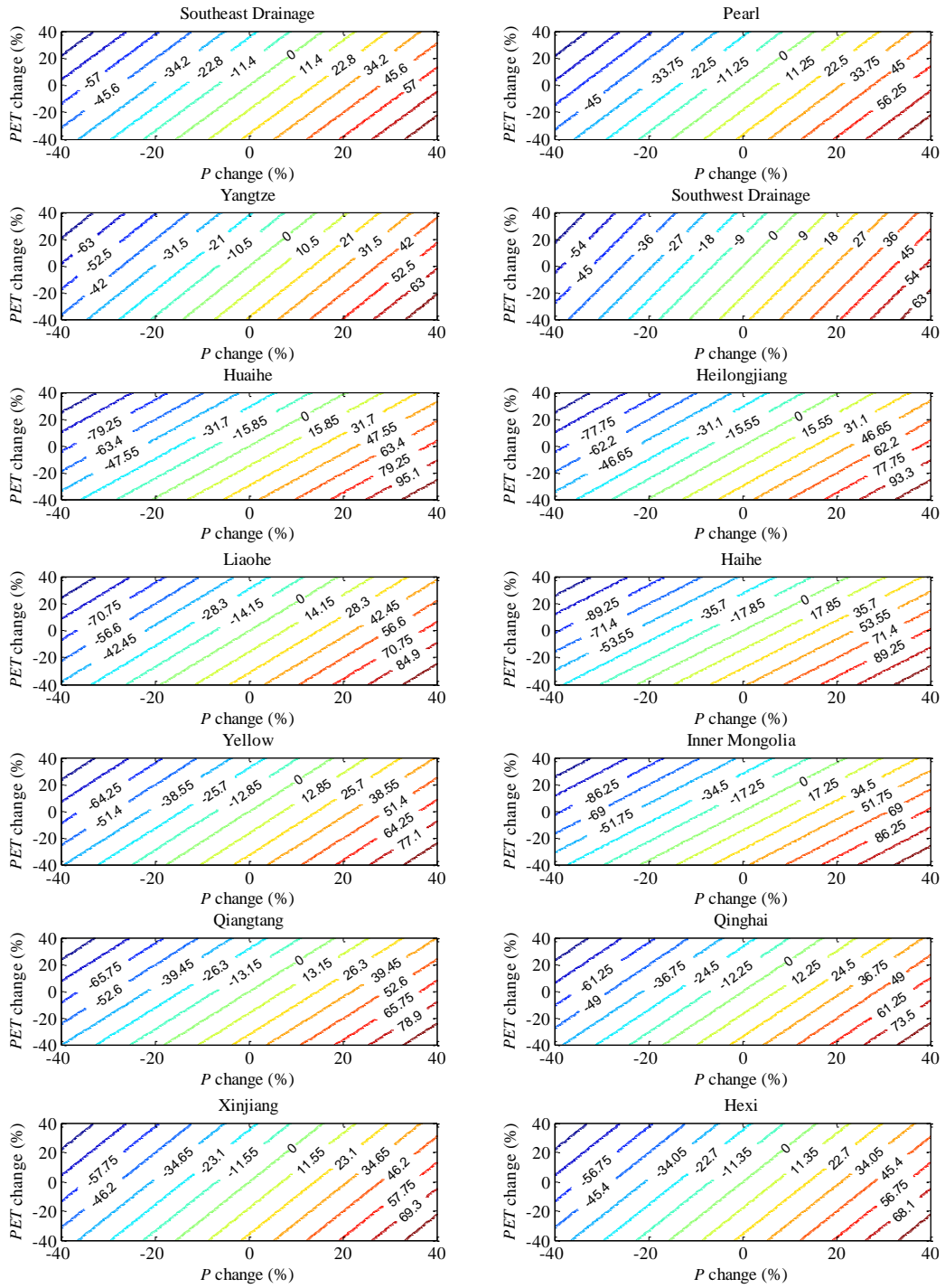
708

709

710

711

712



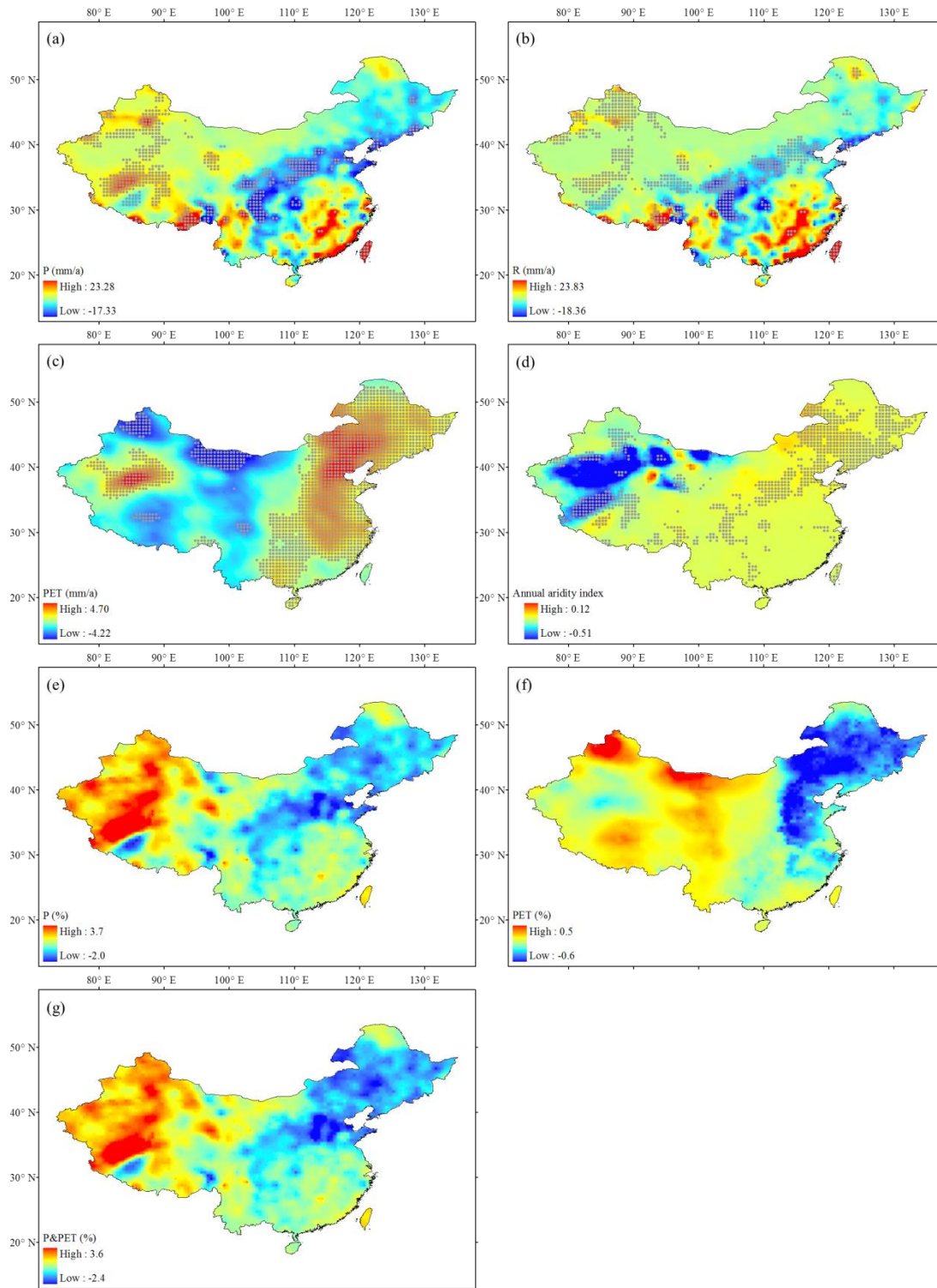
713

714 **Figure 7.** Contour plot of percentage R change due to the changes in P and PET for the 14 river basins.

715 The P elasticity and PET elasticity of R are estimated based on Equation (2).

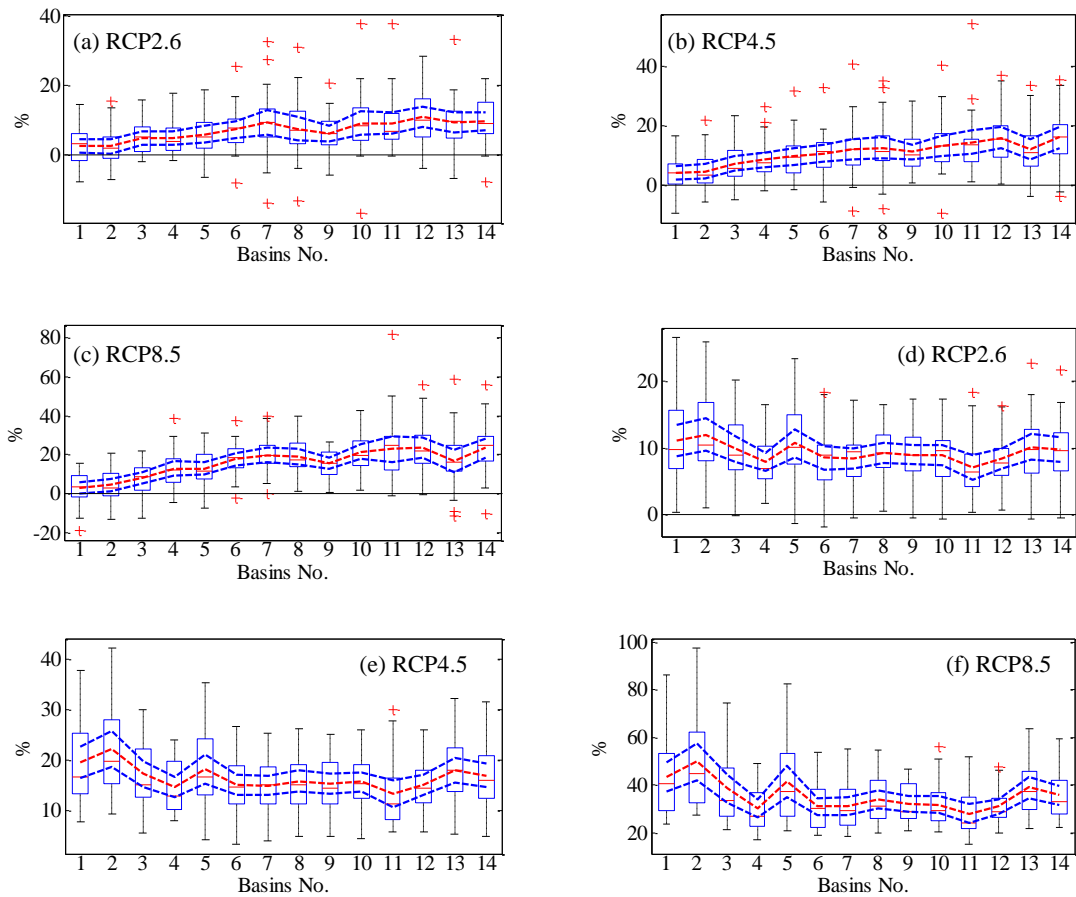
716

717



718

719 **Figure 8.** Trend magnitudes in annual time series of (a) P , (b) R , (c) PET , and (d) aridity index for the
 720 period 1960–2008 and spatial distributions of the contributions (unit: $\% \text{ yr}^{-1}$) of (e) P , (f) PET , and (g)
 721 climate (i.e. P & PET) to R in China for the period 1960–2008. The trend magnitudes are estimated by
 722 the Sen’s method. Grey dots are shown as statistically significant positive/negative trends ($p < 0.05$).



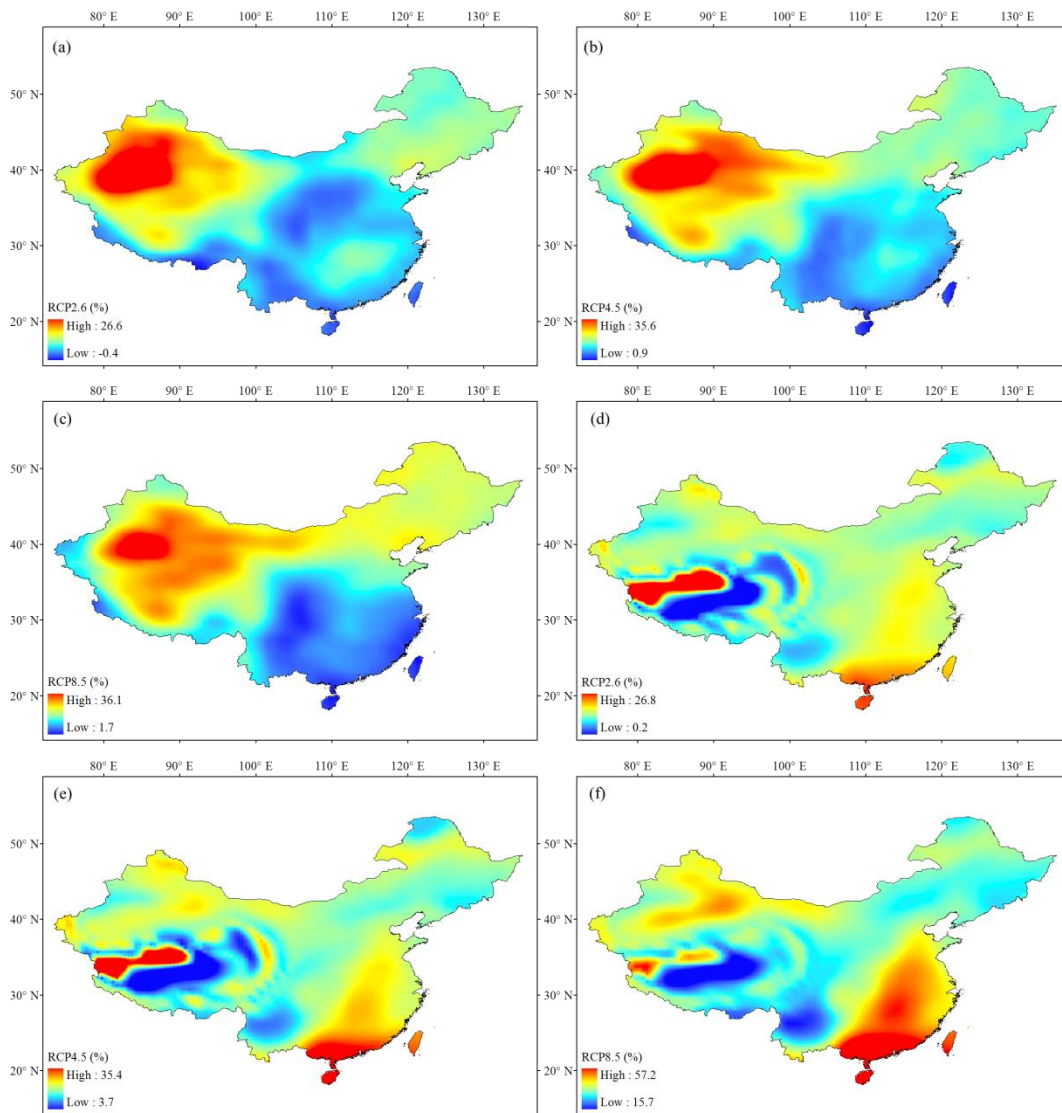
723

724 **Figure 9.** Box plots of relative change (%) in mean annual P under (a) RCP2.6, (b) RCP4.5, and (c)
 725 RCP8.5 scenarios and in mean annual PET under (d) RCP2.6, (e) RCP4.5, and (f) RCP8.5 scenarios
 726 calculated from 28 CMIP5 models in 14 basins for the period 2071–2100 (relative to the baseline 1971–
 727 2000). The boxes denote the interquartile model spread (range between the 25th and 75th quantiles),
 728 with the horizontal line indicating the ensemble median and the whiskers showing the extreme range of
 729 the 28 CMIP5 model simulations. Red dotted lines denote the average values of the multi-model
 730 ensemble. Blue dotted lines denote the 95 % significance levels range of the average values of the
 731 multi-model ensemble. The basin number is consistent with that given in Figure 1.

732

733

734



735

736 **Figure 10.** The CMIP5 multi-model ensemble median relative change (%) in mean annual P under (a)
 737 RCP2.6, (b) RCP4.5, and (c) RCP8.5 scenarios and in mean annual PET under (d) RCP2.6, (e) RCP4.5,
 738 and (f) RCP8.5 scenarios in China for the period 2071–2100 (relative to the baseline 1971–2000).

739

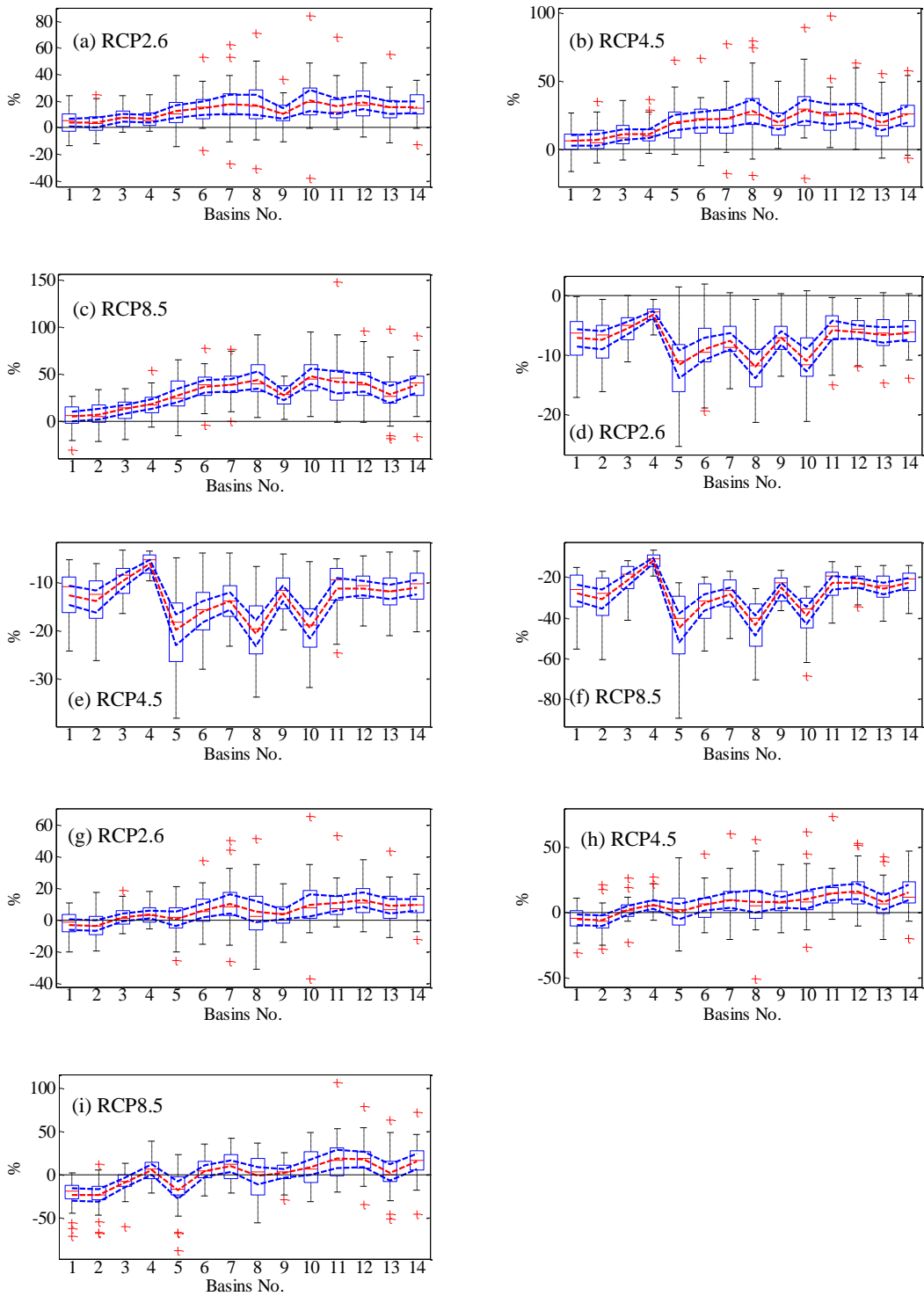
740

741

742

743

744



745

746 **Figure 11.** Box plots of relative change (%) in the contributions of annual P to R under (a) RCP2.6, (b)
 747 RCP4.5, and (c) RCP8.5 scenarios, in the contributions of annual PET to R under (d) RCP2.6, (e)
 748 RCP4.5, and (f) RCP8.5 scenarios, and in the contributions of climate to R under (g) RCP2.6, (h)
 749 RCP4.5, and (i) RCP8.5 scenarios calculated from 28 CMIP5 models in 14 basins for the period 2071–
 750 2100 (relative to the baseline 1971–2000). The boxes denote the interquartile model spread (range
 751 between the 25th and 75th quantiles) with the horizontal line indicating the ensemble median and the
 752 whiskers showing the extreme range of the 28 CMIP5 model simulations. Red dotted lines denote the

753 average values of the multi-model ensemble. Blue dotted lines denote the 95% significance levels range
754 of the average values of the multi-model ensemble. The basin number is consistent with that given in
755 Figure 1.

756

757

758

759

760

761

762

763

764

765

766

767

768

769

770

771

772

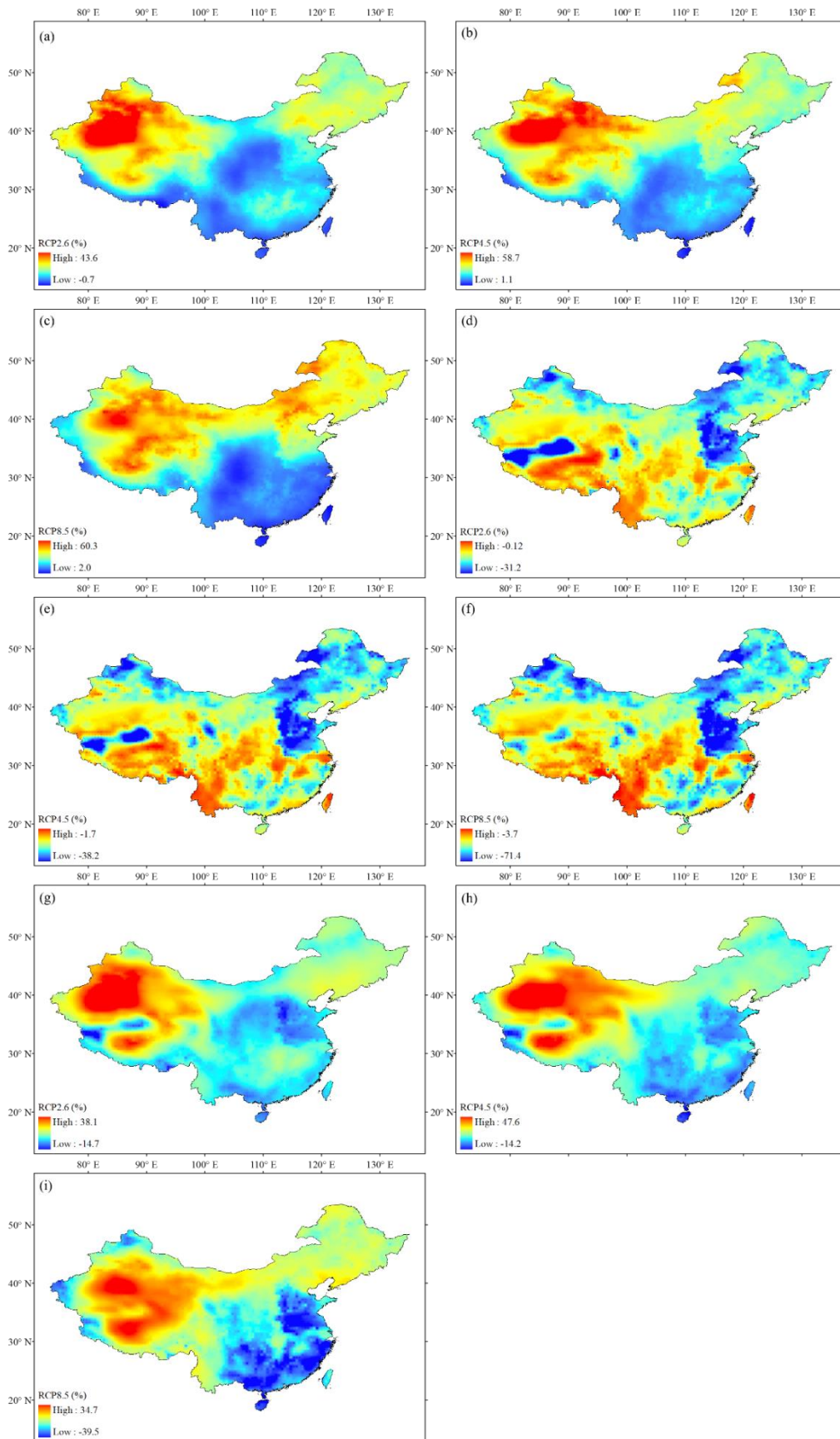
773

774

775

776

777



778

779 **Figure 12.** The CMIP5 multi-model ensemble median relative change (%) in the contributions of
 780 annual P to R under (a) RCP2.6, (b) RCP4.5, and (c) RCP8.5 scenarios, in the contributions of annual
 781 PET to R under (d) RCP2.6, (e) RCP4.5, and (f) RCP8.5 scenarios, and in the contributions of climate

782 to R under (g) RCP2.6, (h) RCP4.5, and (i) RCP8.5 scenarios in China for the period 2071–2100
783 (relative to the baseline 1971–2000).

784

785

786

787

788

789

790

791

792

793

794

795

796

797

798

799

800

801

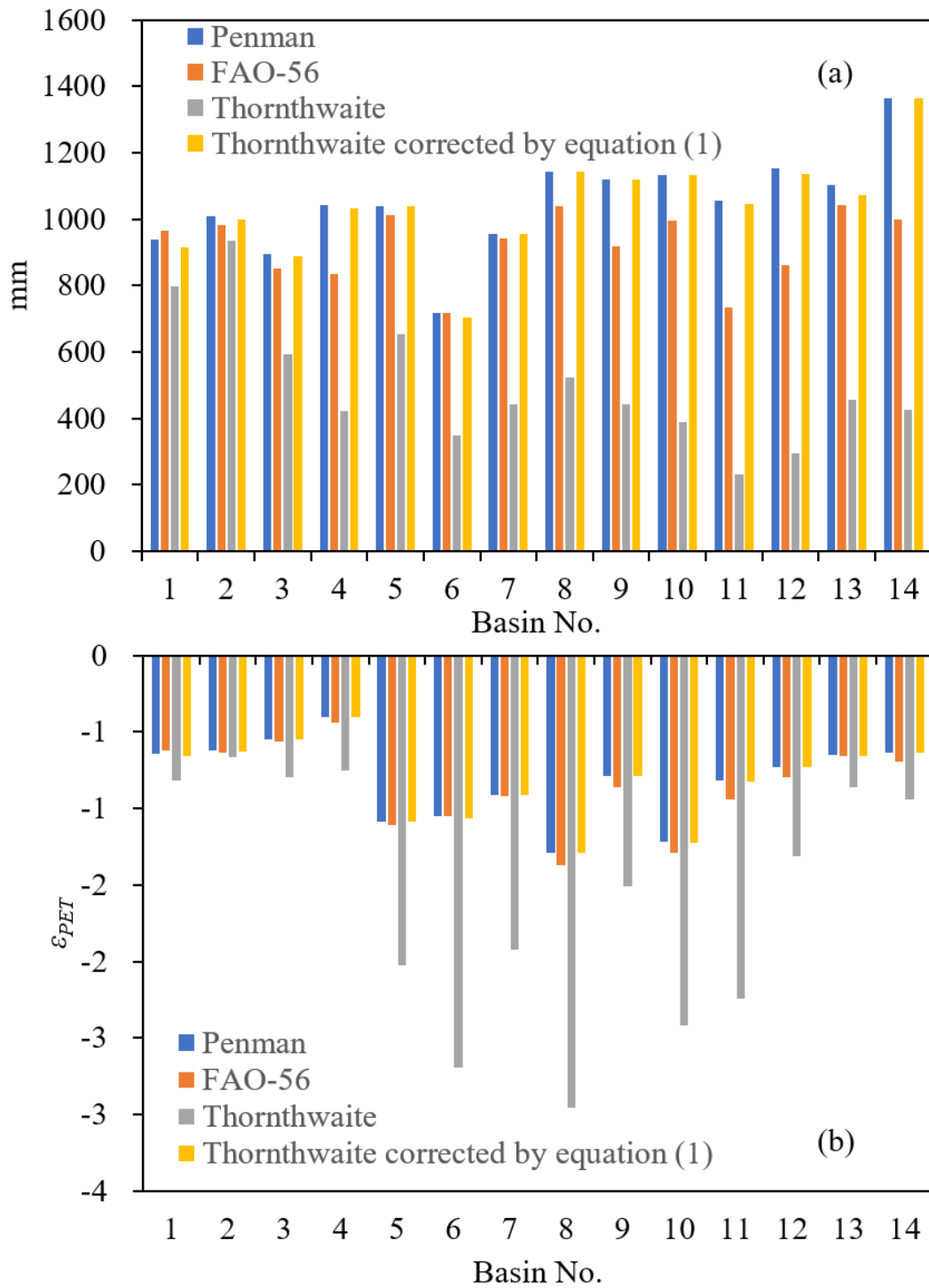
802

803

804

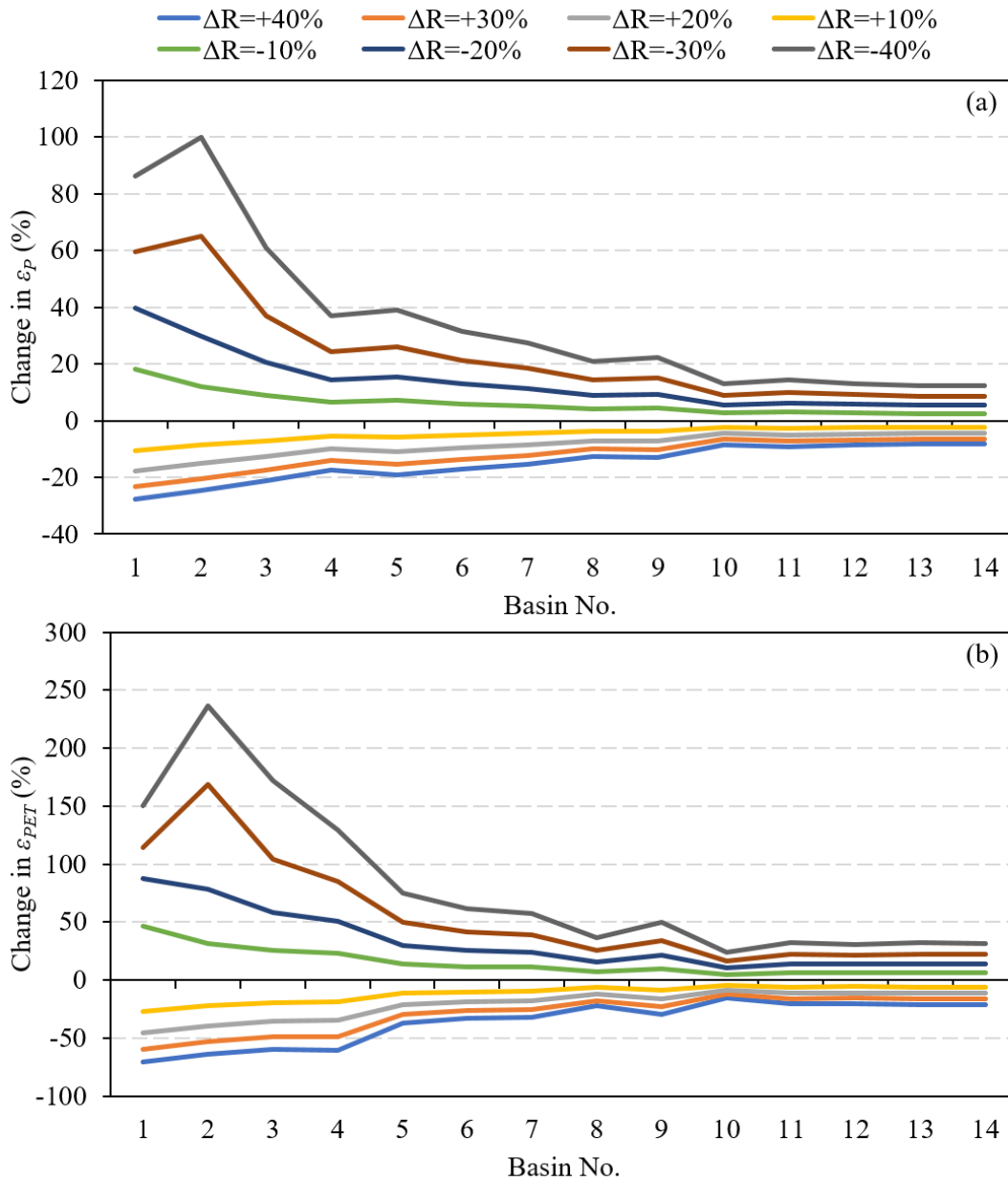
805

806



807
 808 **Figure 13.** (a) Mean annual PET calculated from the four methods for the 14 river basins of China
 809 during the period 1960–2008. (b) PET elasticity calculated from Equation (2) based on the four PET
 810 data for the 14 river basins of China during the period 1960–2008. The basin number is consistent with
 811 that given in Figure 1.

812



813

814 **Figure 14.** Comparison of changes in (a) P elasticity and (b) PET elasticity in response to changes in R

815 for the 14 river basins of China. The basin number is consistent with that given in Figure 1.

816